Cell Communication and Signaling

RESEARCH

Open Access

Nesfatin-1 enhances vascular smooth muscle calcification through facilitating BMP-2 osteogenic signaling

Xue-Xue Zhu[1,2†], Xin-Yu Meng[1†], Guo Chen[1†], Jia-Bao Su[3†], Xiao Fu[1], An-Jing Xu[1], Yao Liu[4], Xiao-Hui Hou[4], Hong-Bo Qiu[1], Qing-Yi Sun[1], Jin-Yi Hu[1], Zhuo-Lin Lv[1], Hai-Jian Sun[1,5], Hai-Bin Jiang[6*], Zhi-Jun Han[7*], Jian Zhu[8*] and Qing-Bo Lu[8*]

Abstract

Vascular calcification (VC) arises from the accumulation of calcium salts in the intimal or tunica media layer of the aorta, contributing to higher risk of cardiovascular events and mortality. Despite this, the mechanisms driving VC remain incompletely understood. We previously described that nesfatin-1 functioned as a switch for vascular smooth muscle cells (VSMCs) plasticity in hypertension and neointimal hyperplasia. In this study, we sought to investigate the role and mechanism of nesfatin-1 in VC. The expression of nesfatin-1 was measured in calcified VSMCs and aortas, as well as in patients. Loss- and gain-of-function experiments were evaluated the roles of nesfatin-1 in VC pathogenesis. The transcription activation of nesfatin-1 was detected using a mass spectrometry. We found higher levels of nesfatin-1 in both calcified VSMCs and aortas, as well as in patients with coronary calcification. Loss-of-function and gain-of-function experiments revealed that nesfatin-1 was a key regulator of VC by facilitating the osteogenic transformation of VSMCs. Mechanistically, nesfatin-1 promoted the de-ubiquitination and stability of BMP-2 via inhibiting the E3 ligase SYTL4, and the interaction of nesfatin-1 with BMP-2 potentiated BMP-2 signaling and induced phosphorylation of Smad, followed by HDAC4 phosphorylation and nuclear exclusion. The dissociation of HDAC4 from RUNX2 elicited RUNX2 acetylation and subsequent nuclear translocation, leading to the transcription upregulation of OPN, a critical player in VC. From a small library of natural compounds, we identified that Curculigoside and Chebulagic acid reduced VC development via binding to and inhibiting nesfatin-1. Eventually, we designed a mass spectrometry-based DNA-protein interaction screening to identify that STAT3 mediated the transcription activation of nesfatin-1 in the context of VC. Overall, our study demonstrates that

†Xue-Xue Zhu, Xin-Yu Meng, Guo Chen and Jia-Bao Su contributed equally to this work.

*Correspondence:
Hai-Bin Jiang
jambo777@163.com
Zhi-Jun Han
zjhan1125@163.com
Jian Zhu
drzhujian@hotmail.com
Qing-Bo Lu
bonnielqb@yeah.net

Full list of author information is available at the end of the article

nesfatin-1 enhances BMP-2 signaling by inhibiting the E3 ligase SYTL4, thereby stabilizing BMP-2 and facilitating the downstream phosphorylation of SMAD1/5/9 and HDAC4. This signaling cascade leads to RUNX2 activation and the transcriptional upregulation of MSX2, driving VC. These insights position nesfatin-1 as a potential therapeutic target for preventing or treating VC, advancing our understanding of the molecular mechanisms underlying this critical cardiovascular condition.

Keywords Vascular calcification, VSMC, Nesfatin-1, STAT3, BMP-2

Introduction

Vascular calcification (VC) is a prevalent characteristic of various diseases, including chronic kidney disease (CKD), diabetes, hypertension, atherosclerosis, and aging [1, 2]. VC, especially in the tunica media, is believed to be an independent risk factor for cardiovascular diseases and events [3, 4]. The severity of VC escalates with disease progression in patients with end-stage renal disease [5]. It is well known that the transition of vascular smooth muscle cells (VSMCs) from a contractile to an osteogenic phenotype is widely accepted as a significant contributor to VC development [6]. During this transition, there is a notable loss of VSMC contractile markers, such as smoothelin, calponin, and smooth muscle 22a [7]. Simultaneously, there is an increased expression of genes associated with an osteogenic profile, including alkaline phosphatase (ALP), osteopontin, osteocalcin, bone morphogenetic protein 2 (BMP-2), core binding factor a 1, and osterix [3, 8]. A delicately balanced interplay between inducers and inhibitors probably elaborates the occurrence of VC under pathological conditions. These osteogenic markers are critical for the initiation and progression of calcification within VSMCs, leading to the deposition of calcium phosphate crystals in the extracellular matrix. As VSMCs undergo calcification, they contribute directly to the overall VC observed in various cardiovascular diseases. The calcified VSMCs lose their contractile function, contributing to the stiffening of the vessel wall and the development of atherosclerotic plaques, which further exacerbate VC. Moreover, the calcification of VSMCs can disrupt the structural integrity of the vascular wall, making it more prone to rupture, thereby increasing the risk of adverse cardiovascular events. The pathogenesis of VC has implicated numerous mechanisms, such as apoptosis, loss of matrix Gla protein (MGP), mineral imbalance, or inflammation [9–11]. Nevertheless, the comprehensive understanding of the molecular and cellular mechanisms underlying VC is still incompletely understood.

Nesfatin-1, an anorexigenic neuropeptide derived from nucleobindin-2 precursor (NUCB2), plays a significant role in regulating food intake, hunger and satiety, glucose and lipid metabolism, affective disorders, blood pressure, gut motility, energy expenditure, and stress response [12]. Studies have shown that nesfatin-1 is ubiquitously expressed in both central and peripheral regions of the body, and its levels are influenced by hunger and refeeding [13]. As a versatile biomolecule, nesfatin-1 plays a significant role in the diagnosis and treatment of various diseases, such as coronary artery disease [14], multiple sclerosis [15], depression [16], hypertension [17], and type 2 diabetes mellitus [18]. Studies have indicated that nesfatin-1 is associated with inhibiting lipid-related disorders, as it diminishes fat accumulation and enhances lipid decomposition in lipid metabolism [19]. Previously, we found that chronic infusion of nesfatin-1 induced hypertension and vascular remodeling in rats by facilitating VSMC phenotypic switching and proliferation [20]. Downregulation of nesfatin-1 ameliorated neointima formation following carotid injury in rats through downregulating matrix metalloproteinases and upregulating peroxisome proliferator-activated receptor γ (PPARγ) in VSMCs [21]. Despite the potential role of nesfatin-1 in VSMC functions, little is known with the respect of the function of nesfatin-1 in VC development. Therefore, we used in vitro, ex vivo, and in vivo models to study the role and underlying molecular mechanism of nesfatin-1 in VC. Our results showed that nesfatin-1 promoted the development of VC by facilitating the osteogenic transdifferentiation of VSMCs. Molecular and cellular studies revealed that nesfatin-1 disrupted the interaction of BMP-2 with the E3 ligase SYTL4, leading to the overactivation of BMP-2 signaling. Drug screening experiments found that Curculigoside and Chebulagic acid alleviated VC via binding to and inhibiting nesfatin-1. A mass spectrometry-based DNA-protein interaction screening showed that STAT3 was responsible for the upregulation of nesfatin-1 in the context of VC. Overall, our results highlighted the functional role of nesfatin-1 in VC, and nesfatin-1 may be taken as a promising therapeutic target for VC.

Materials and methods

Chemicals and reagents

Fetal bovine serum (FBS), trypsin, 1% penicillin/streptomycin and DMEM medium were purchased from Hyclone Laboratories (South Logan, UT, USA). Sodium phosphate (Pi) and glycerophosphoric acid disodium (β-GP) were purchased from Sigma-Aldrich (St Louis, MO, USA). Western and IP Lysis Buffer, Proteinase inhibitor and Calcineurin inhibitor were bought from Beyotime Biotechnology (Shanghai, China). Recombinant

human BMP receptor 1 A (BMPR-IA) was obtained from R&D Systems (Minneapolis, MN, USA). A commercial kit for measurement of calcium was purchased from Jiancheng Bioengineering Institute (Nanjing, China), and ALP activity kit was purchased from Abbkine (Beijing, China). Alizarin Red S staining solution (pH4.2, 1%) and Von Kossa assay kit were obtained from Solarbio (Beijing, China). MG132, Chloroquine, Pronase E, Curculigoside, Chebulagic acid, and cyclohexane (CHX) were purchased from MCE (Shanghai, China). Protein A/G beads were purchased from Santa Cruz (Santa Cruz, USA).

Study population

This study was adhered to the ethical principles outlined in the 1975 Declaration of Helsinki and received prior approval from the Ethics Committee of Nanjing Medical University (20180705-K048). The checklist of STROBE statement used for this study was provided in the Supplementary material online, Text S2. Upon obtaining the written informed consent, patients were asked to complete a brief questionnaire and their medical records were reviewed anonymously. A total of 102 consecutive patients suspected of coronary artery disease (CAD) and who had undergone coronary calcium assessment via multi-detector row CT were included in the study (Table S1). The calcium scan was performed for risk assessment purposes in individuals deemed to have an increased likelihood of future CAD events based on traditional risk factors or those experiencing atypical chest pain. Individuals with acute cardiovascular or cerebrovascular ischemic diseases, diabetes mellitus, congestive heart failure, peripheral artery disease, familial hyperlipidemia, severe hepatic dysfunction, renal insufficiency, potential infectious or inflammatory diseases, carcinoma, a history of percutaneous coronary intervention and/or coronary artery bypass grafting, atrial fibrillation, acute coronary syndrome (ACS) episode within the last three months, immunologic disorders, corticosteroid therapy, or who were either over 80 years old or under 18 years old were excluded from this study. The Agatston scores were determined by a skilled image analyst following established criteria. Based on the coronary artery calcium scores, participants were categorized into four groups: 0–10 (no calcification), 11 to 100 (mild calcification), 101 to 400 (moderate calcification), and over 400 (severe calcification) [22, 23]. Fasting blood samples were obtained in the morning prior to the CT scan and refrigerated at 4 °C for up to 4 h before processing. The samples were collected using sodium heparin Vacutainers from Becton-Dickinson. After centrifugation at 2000 × g for 15 min, the serum was stored at -80 °C until analysis. The laboratory data were measured and recorded.

Animals

Male C57BL/6J mice, aged 16 weeks, were procured from spfbiotech Co. Ltd (Nanjing, China). All animal experiments were in compliance with the guidelines from Directive 2010/63/EU of the European Parliament and approved by the Care and Use of Laboratory Animals of China Pharmaceutical University (202101006). All mice were caged under a humidity and temperature-controlled environment on a 12-h light and dark cycle, with unrestricted access standard chow and clean water. VC mice were induced by administration of vitamin D3 (VD3) as previously described [24–26]. In short, the mice were subjected to subcutaneous injection of vitamin D3 (VD3, 5.5×10^5 U/kg, Sigma, C1357) once a day for three times. All mice were maintained on a normal diet for 6 weeks. The mice were anesthetized and euthanized to collect blood and aorta samples after 6 weeks of VD3 injection. To specifically knock down nesfatin-1 in VSMCs, recombinant AAV serotype 9 (AAV9) gene transfer vectors-mediated nesfatin-1 shRNA and negative control shRNA under the guidance of SM22α promoters were injected into mice through the tail vein (2×10^{11} vector genomes). The oligonucleotide sequence of mouse nesfatin-1 shRNA was as follows: 5′-GGATCATCCAAGT ACAGTA-3′, and the scrambled shRNA oligonucleotide sequence was as follows: 5′-CAACACTAGTTGACATG TA-3′ [27]. AAV9 vectors carrying nesfatin-1 shRNA or the scramble control shRNA was generated by Packgene (Guangzhou, China). One week after injection of AAV9 vectors, the mice were then injected to VD3 (5.5×10^5 U/kg) once a day for three times as mentioned above. Full-length mouse nesfatin-1 complementary DNA (cDNA) was cloned into the pAAV-CMV-EGFP-P2A-3xFLAG-WPRE plasmid. AAV9 vectors carrying the plasmid (AAV9-cmv-nesfatin-19 or the scramble control (AAV-cmv-GFP) under the control of SM22α promoters was also generated by the Packgene (Guangzhou, China). To determine the role of VSMC-specific overexpression of nesfatin-1 in the occurrence and development of VC, the mice were injected with the indicated virus (2×10^{11} plaque-forming units per kilogram per mouse) via tail vein, respectively. One week after VSMC-specific overexpression of nesfatin-1, VD3-induced mice were constructed. The mice were intraperitoneally injected with Curculigoside (30 mg/kg) or Chebulagic acid (30 mg/kg) every other day for 6 weeks during the induction of VC. For euthanasia, animals were anesthetized with 5% isoflurane, anesthesia was confirmed via tail pinch, and then sacrificed by cervical dislocation.

Cell culture

Primary VSMCs were obtained from the thoracic aortic arteries of Sprague-Dawley rats (150–180 g) using enzymatic digestion methods as we described previously [28].

For the experiments, VSMCs at passages 5 to 8 were utilized. VSMCs were cultured in DMEM supplemented with 10% FBS, 100 U/mL penicillin, and 100 mg/mL streptomycin at 37 °C in a 95% air and 5% CO_2 incubator. To initiate calcification, confluent VSMCs were exposed to medium containing β-GP (5 mM) and Ca^{2+} (2.5 mM) for two consecutive weeks, following established protocols. In addition, VSMCs were cultured in DMEM containing Na_2HPO_4/NaH_2PO_4 solution (2.6 mM) for 12 days to induce calcification [29]. The control VSMCs were treated with DMEM containing 10% FBS, 100 U/mL penicillin, and 100 μg/mL streptomycin, but without Na_2HPO_4/NaH_2PO_4 solution, and the medium was also refreshed every 3 days. A lentiviral vector expressing nesfatin-1 shRNA or the negative control shRNA was constructed and transduced into VSMCs at a multiplicity of infection (MOI) of 50 at 3 days before high Pi treatment. Three shRNAs were designed and listed as follows: nesfatin-1 shRNA1, 5′-GACTGAGAATGCTCATCAA-3′ (forward), 5′-TTGATGAGCATTCTCAGTC-3′ (reverse); nesfatin-1 shRNA2, 5′-GGACTTAGTAAGTCACAAA-3′ (forward), 5′-TTTGTGACTTACTAAGTCC-3′ (reverse); nesfatin-1 shRNA3, 5′-GGTGGAAAGTGCAAGGATA-3′ (forward), 5′-TATCCTTGCACTTTCCACC-3′ (reverse). The sequences for control shRNA were listed as follows: 5′-TTTCTCTTCACTCAATAAA-3′ (forward), 5′-TTTATTGAGTGAAGAGAAA-3′ (reverse). Likewise, a pLVX-IRES-Puro lentiviral vector carrying nesfatin-1 gene or its negative control lentivirus was constructed and transduced into VSMCs (MOI=50) 3 days before high Pi stimulation.

Ex vivo vascular tissue culture

Mice aortic arteries were dissected under sterile conditions from 16-week-old male C57BL/6J mice. After removing the adventitia and endothelium, the vessels were cut into 2–3 mm rings and placed in Dulbecco's modified Eagle's medium (DMEM) (Gibco) containing 10% FBS with or without 3.8 mM inorganic phosphate for 7 consecutive days, and the medium was changed every 2 days. The aortic rings were transfected with lentivirus-mediated nesfatin-1 shRNA or nesfatin-1 overexpression plasmid for 7 days at a multiplicity of infection (MOI) of 50 in the absence or presence of 3.8 mM inorganic phosphate. Seven days later, the aortic rings were harvested.

Transfection of VSMCs

Upon 50–60% confluence, VSMCs were cultured in serum-free DMEM and transfected with lentivirus-mediated control shRNA (forward, 5′-TTTCTCTTCACTCAATAAA-3′; reverse, 5′-TTTATTGAGTGAAGAGAAA-3′), SYTL4 shRNA1 (forward, 5′-GCGTGTAAGTTGTCTACAA-3′; reverse, 5′-TTGTAGACAACTTACACGC-3′), SYTL4 shRNA2 (forward, 5′-GGAAGTAGATGATCTAGTA; reverse, 5′-TACTAGATCATCTACTTCC-3′), SYTL4 shRNA3 (forward, 5′-GCTATAAGTTAGAAGGTTA-3′; reverse, 5′-TAACCTTCTAACTTATAGC-3′), SYTL4 overexpression plasmid (TL712429, Origene), STAT3 overexpression plasmid (RR206813L3, Origene), K278A mutation plasmid (Genepharm), K287A mutation plasmid (Genepharm), K290 mutation plasmid (Genepharm), con siRNA (sc-108080, Santa Cruz), STAT3 siRNA (sc-270027-V, Santa Cruz) (10 μL/mL, multiplicity of infection: 50) according to the manufacturer's instructions. After transfection for 6 h, the DMEM containing 10% FBS was replaced.

Plasmid construction and transfection

Sequences encoding full-length nesfatin-1 and BMP-2 were cloned into pcDNA3.1-hemagglutinin (HA) vectors, leading to the pcDNA3.1-HA-nesfatin-1 and pcDNA3.1-HA-BMP-2 plasmids. Sequences encoding full-length MARCHF1, SYTL4, ZEB2, MARCHF3 and MARCHF8 were cloned into pcDNA3.1-Flag vectors, yielding the pcDNA3.1-Flag-MARCHF1, pcDNA3.1-Flag-SYTL4, pcDNA3.1-Flag- ZEB2, pcDNA3.1-Flag-MARCHF3, pcDNA3.1-Flag- MARCHF8 plasmids. Sequences encoding full-length nesfatin-1 and BMP-2 were separately cloned into pcDNA3.1-Flag and pcDNA3.1-hemagglutinin (HA) vectors, generating the pcDNA3.1-Flag-Nesfatin-1 and pcDNA3.1-HA-BMP-2. Similarly, pcDNA3.1-Flag-BMP-2 and pcDNA3.1-HA-nesfatin-1 plasmids were obtained by cloning the specified cDNA segments of BMP-2 and nesfatin-1 into pcDNA3.1-Flag and pcDNA3.1-HA, respectively. For pcDNAc3.1-Flag-Nesfatin-1 and Nesfatin-1 fragments (residues 1–86, 1-368, 87–461, 148–461 and 369–461) was cloned into the pcDNA3.1-Flag and psi-Flag vectors, respectively. For pcDNA3.1-Flag-BMP-2 and BMP-2 fragments (residues 1-395, 1-135, 1-283, 136–395, 200–395, and 284–395) created by cloning the encoding region of the human BMP-2 into pcDNA3.1-HA. Human Embryonic Kidney 293-T (HEK 293T) cells were maintained in Dulbecco's Modified Eagle's Medium (DMEM; Gibco, Carlsbad, CA, USA) supplemented with 10% fetal bovine serum (FBS; Gibco, Carlsbad, CA, USA) and 1% double antibiotics (penicillin-streptomycin solution, Gibco, Carlsbad, CA, USA) at 37 °C in a 5% CO_2 environment. After transfecting the specific plasmids in HEK 293-T cells, 500 μg of protein samples underwent incubation with the antibody-coupled resin for 2 h. Subsequently, the protein-antibody complexes were eluted using a 50 μl elution buffer following proper mixing and washing. The eluted protein samples were then analyzed via immunoblotting using the respective antibodies.

Immunofluorescence staining

Immunofluorescence staining was utilized to detect nesfatin-1, α-SMA, RUNX2 and HDAC4 in mouse aorta sections or VSMCs. Briefly, the collected VSMCs were fixed with 4% paraformaldehyde solution for 30 min, and then samples were washed in PBS 3 times. Or the 5-μm aorta sections were deparaffinized and rehydrated. Next, samples were permeabilized using 0.1% Triton-X. After three PBS washes, VSMCs or aorta sections were incubated with 5% BSA for 30 minutes. Following this, the primary antibodies against nesfatin-1 (26712-1-AP, Proteintech), α-SMA (ab7817, Abcam), RUNX2 (ab192256, Abcam, rabbit), and HDAC4 (ab12172, Abcam, rabbit), respectively, were incubated overnight at 4°C. Alexa Fluor 488 goat anti-mouse IgG (A11029, invitrogen) and Alexa Fluor 594 goat anti-rabbit IgG (A11012; invitrogen) were incubated for 1 h at room temperature. 4′,6-diamidino-2-phenylindole (DAPI) staining was incubated for 10 min at room temperature. Imaging was performed usingfluorescence microscope (Nikon, Japan).

RT-PCR

The Trizol reagent was used to extract total RNA in VSMC cells and aortic tissues according to the manufacturer's protocols. Equal amount of RNA (1 μg) was reverse transcribed by Hifair® III 1st Strand cDNA Synthesis SuperMix (Yeasen Biotechnology, Shanghai, China). Next, the real-time PCR was conducted by the Applied Biosystems QuantStudio 3 (ThermoFisher, USA) using SYBR Green PCR master mix (Yeasen Biotechnology, Shanghai, China). The $2^{-\Delta\Delta Ct}$ method β-actin was utilized to calculate mRNA expression normalized to β-actin. The primers were described in Table S2-3.

Nuclear/cytoplasmic extraction

At collection time points, culture medium was removed and then VSMCs were washed with 1× PBS for 3 times. The nuclear and cytoplasmic protein lysate extraction of VSMCs was performed using the Nuclear Protein Extraction Kit (Beyotime Biotechnology, Shanghai, China) according to the manufacturer's recommendations.

Western blotting and co-immunoprecipitation (co-IP)

Samples were lysed using western and IP Lysis Buffer (Beyotime, Shanghai, China) containing Proteinase inhibitor (Beyotime, Shanghai, China). Equal amounts of proteins were separated by 8–12% sodium dodecyl sulfate-polyacrylamide gel (SDS-PAGE) gel, electrotransferred to polyvinylidene difluoride (PVDF, Millipore Darmstadt, Germany) membranes, and blocked with 5% non-fat milk. After that, blots were incubated with indicated primary antibodies for overnight at 4℃ followed by exposure of horseradish peroxidase (HRP)-coupled secondary antibodies. The following antibodies were used: anti-nesfatin-1 antibody (#26712-1-AP, Proteintech), anti-RUNX2 antibody (#12556S, Cell Signaling Technology or 82636-2-RR, Proteintech), anti-BMP-2 antibody (#ER80602, Huabio), anti-α-SMA antibody (#14395-1-AP, Proteintech), anti-SM22α antibody (#10493-1-AP, Proteintech), anti-HDAC4 antibody (#7628S, Cell Signaling Technology), anti-p-Smad antibody (#13820, CST), anti-T-Smad antibody (#6944, CST), anti-Msx2 antibody (#orb415625, Biorbyt), anti-Lamin B1 (#12987-1-AP, Proteintech), anti-HA (81290-1-RR, Proteintech), anti-Flag antibody (66008-4-Ig, Proteintech), anti-β-actin (#4970, CST), anti-His antibody, (#66005-1-Ig Proteintech), anti-STAT3 (#10253-2-AP, Proteintech), anti-HDAC4 antibody (#7628, CST), anti-p-HDAC4 antibody (Ser246, #bs-10325R, Bioss), anti-Ub antibody (#10201-2-AP, Proteintech), anti-GAPDH antibody (#60004-1-Ig, Proteintech), Anti-Acetylated-Lysine antibody (#9441, CST), anti-SYTL4 antibody (#12128-1-AP, Proteintech), anti-STAT3 antibody (#9139, CST), anti-β-tubulin (#M05613-6, Boster), HRP-linked anti-rabbit IgG (SA00001-2, Proteintech), HRP-linked anti-mouse IgG (SA00001-1, Proteintech). For co-IP experiments, the collected cells and tissues were lysed using Western and IP lysis buffer (Beyotime, Shanghai, China) on ice or at 4℃ for 30 min. Then, the samples were centrifuged at 12,000 g for 15 min and the supernatant were collected. The lysates were immunoprecipitated with 1 μg of the indicated antibodies against RUNX2 (82636-2-RR, Proteintech) or BMP-2 (sc-137087, Santa Cruz Biotechnology) at 4℃ for 2 h and 20 μl of protein A/G beads at 4℃ overnight. After that, the complexes were washed, loaded and detected using western blotting. The bands were imaged using an enhanced chemiluminescence (ECL, Biosharp, Shanghai, China) solution and the band densities were analyzed using ImageJ software.

Von Kossa assay

To examine aorta calcification, paraffin-embedded Sect. (5 μm) were deparaffinized, rehydrated and rinsed rapidly in double distilled water. The vascular tissue sections were then incubated with 5% silver nitrate solution and exposed to ultraviolet light for 1 h until color development was complete. Next, the slides were incubated with 5% sodium thiosulfate and washed with double distilled water. The slides were photographed by microscopy (Nikon, Japan). Calcified nodules were stained brown to black.

Alizarin red staining

Cultured VSMCs were washed with 4 °C PBS 3 times, and then fixed in 4% paraformaldehyde in PBS for 20 min. The paraformaldehyde was removed and the cells were washed in distilled water 3 times (2 min each wash). Or the 5-μm aortic slices were deparaffinized and

rehydrated. The fixed cells or sections were then exposed to Alizarin red staining solution (pH 4.0, 1%) for 30 min at room temperature. A reddish color was photographed to demonstrate the calcification by microscopy (Nikon, Japan).

Calcium and ALP quantification

VSMCs or aortic tissues with no adventitia were decalcified with 0.6 mol/L HCl at 4 °C for 24 h, and the supernatant was collected. Calcium levels were determined using a commercial kit (Nanjing Jiancheng Bioengineering Institute, Nanjing, China) following the manufacturer's instructions. VSMCs or aortic tissues were lysed with 0.1 M NaOH/0.1% SDS and calcium content was normalized to total protein concentration, determined by the BCA assay (Abbkine, China). ALP quantification was performed by equilibrating VSMCs or aortic tissues with Extraction Buffer on ice, followed by collecting the supernatant after centrifugation in a microfuge at 10,000 rpm for 10 min at 4℃. ALP activity was analyzed using a commercial assay kit (Nanjing Jiancheng Bioengineering Institute, Nanjing, China) and results were normalized to total protein levels.

Confocal microscopy

The interaction of BMP-2 with nesfatin-1 was also observed using laser scanning confocal microscope in VSMCs. VSMCs were fixed using 4% paraformaldehyde, then blocked with 5% bovine serum albumin for 1 h at room temperature. Subsequently, they were incubated overnight at 4°C with antibodies targeting BMP-2 (primary mouse antibody, 66383-1-Ig, Proteintech, Rosemont, USA rabbit) and nesfatin-1 (primary rabbit antibody, 26712-1-AP, Proteintech, Rosemont, USA rabbit). The next day, samples underwent staining with a mixture of Alexa Fluor 488 goat anti-rabbit IgG (ab150077, Abcam) and Alexa Fluor 594 goat anti-mouse IgG (ab150116, Abcam) secondary antibodies at 37°C for 1 h in the dark environment. The cell nuclei visualized by counterstaining with 4′,6-diamidino-2-phenylindole (DAPI). Imaging was performed using a ZEISS scanning confocal microscope (LSM880 with Airyscan, Germany).

Enzyme-linked immunosorbent assay (ELISA)

The plasma level of nesfatin-1 was measured and quantified using commercially available human nesfatin-1 ELISA kit (No. EK1138, Boster, China) following the manufacturer's protocols. In short, the standards at different concentrations and sample diluent were added into the indicated wells of the ELISA plate under a sealing membrane at 37 ℃ for 90 min. After that, the prepared biotin-coupled anti-human nesfatin-1 antibody was added and incubated at 37 ℃ for 60 min. After three washes, the prepared ABC working solution was added into the appropriate wells at 37 ℃ for 30 min. The plates were washed with the washing buffer for 5 times, followed by the adding of TMB colorimetric solution at 37 ℃ for 30 min. Finally, the termination solution was added for 20 min, and the optical density was measured using the BioTek microplate reader (Winooski, VT, USA). The TMB blank color wells were set as controls. After subtracting the absorbance values of TMB blank color from the absorbance values of all standard and sample samples, draw a curve on a coordinate paper with absorbance values as the vertical axis and concentration as the horizontal axis.

Drug screening

After stimulation by high Pi for 10 days, VSMCs were transfected with nesfatin-1 luciferase reporter gene for 24 h using Lipofectamine 2000 (Invitrogen, Carlsbad, CA, USA), followed by incubated with a small compound library containing 179 phenol compounds (5 μM, Table S4) for another 24 h in the presence and absence of high Pi. Subsequently, the lysates were utilized to determine the activities of firefly luciferase and renilla luciferase through the use of the Luciferase Reporter Gene Assay Kit (Yeasen, China).

Chromatin immunoprecipitation (ChIP) assay

The EZ-CHIPTM Chromatin Immunoprecipitation Kit (Millipore) was employed for the ChIP assay. The cells were fixed with 10% formaldehyde for 10 min and then terminated with glycine. Cell precipitates were collected by centrifugation and lysed with cell lysis solution (Sigma). This resulted in cell nuclear precipitates, which were sonicated to yield sonically sheared cell nuclear lysates. The lysates were then incubated overnight at 4 °C with either control IgG antibody (Proteintech, 30000-0-AP) or STAT3 antibody (Proteintech, 10253-2-AP). Next, the DNA bound to the STAT3 transcription factor was centrifuged, eluted, and extracted using fresh elution buffer. Purified DNA underwent RT-PCR for analysis. The normalized enrichment value was calculated using the difference between the relative value of the immunoprecipitation (IP) and the relative value of the input.

Molecular docking

The AlphaFold2 was used to predict the crystal structure corresponding to nesfatin-1 protein. The protein crystal obtained was processed using the Protein Preparation Wizard module of Schrödinger software, including protein preprocessing, regeneration of native ligand states, optimization of H-bond assignment, protein energy minimization, and removal of waters. The 2D sdf structure file of the compound was processed using the LigPrep module in Schrödinger to generate all its 3D chiral conformations. The SiteMap module in Schrödinger was

used to predict the optimal binding site. Then, the Receptor Grid Generation module in Schrödinger was used to set the most suitable Enclosing box to perfectly wrap the predicted binding site and obtain the active site of the Nesfatin-1 protein. The preprocessed ligand compound was docked with the active site of the Nesfatin-1 protein using molecular docking (flexible docking) in XP mode. The molecular docking complex of the ligand compound with the active site of the nesfatin-1 protein was subjected to MM-GBSA calculation analysis. MM-GBSA dG Bind can approximate the binding free energy between small molecules and proteins. Lower binding free energy values indicate higher stability of ligand-protein binding. The MM-GBSA analysis results are based on MM-GBSA dG Bind.

Mass spectrometry (MS) analysis

Proteomic analysis involved several key steps: preparation of bait oligonucleotides, SNP pulldown, and LC-MS mass spectrometry. Initially, the nesfatin-1 promoter was cloned using desthiolobiotinylated primers. Following the PCR reaction, the oligonucleotides were isolated with chloroform-phenol extraction. Streptavidin C1 Dynabeads (Invitrogen) were then incubated with DNA oligos in DW buffer. After a 1-h blocking step at 4 °C, nuclear extractions from VSMCs were co-incubated with the DNA-beads complex for 2 h on a rotator and eluted with 16 mM biotin. Subsequently, the proteins were ethanol-precipitated and re-solubilized in 8 M urea with 0.5 mM DTT for MS analysis. The obtained liquid chromatography–tandem mass spectrometry (LC-MS/MS) data were analyzed against a UniProtKB human database using the Integrated Proteomics Pipeline (IP2, http://integrated-proteomics.com/). The transcriptional factors were then identified.

Cellular thermal shift assay (CETSA)

CETSA was conducted using M-PER (R) Mammalian Protein Extraction Reagent (Solarbio, Beijing, China) for protein extraction. Cell extracts were incubated with either DMSO or Curculigoside/Chebulagic acid for 1 h at room temperature. Each sample was divided into 7 tubes and heated at a specific temperature for 5 min with gentle mixing. Following centrifugation at 12,000 g at 4 °C for 20 min, the resulting supernatants were analyzed using immunoblotting.

Drug affinity responsive target stability (DARTS)

DARTS assay was carried out following the method described as previously [30, 31]. Cell lysates were treated with either DMSO (vehicle) or Curculigoside, Chebulagic acid for 30 min at room temperature. Subsequently, Pronase was used for digestion for an additional 30 min at room temperature. The samples were then mixed with SDS loading buffer and immediately heated at 98 °C for 10 min before being subjected to immunoblotting.

Statistical analysis

The experimental results, presented as means ± SEM, were analyzed using various statistical tests including Wilcoxon signed-rank test, Student's t test, and one-way or two-way analysis of variance (ANOVA) for comparing numerical variables. Normality of the data was assessed using the Shapiro-Wilk test and quantile-quantile plots. Statistical comparisons were made between two groups using Student's t-test, and among multiple groups using ANOVA/Bonferroni-test. Proportions of categorical variables were compared using Chi-square or Fisher's exact tests. Statistical analysis was carried out using SPSS (version 19.0) or GraphPad Prism (version 7.0) software. A statistical significance level of less than 0.05 was considered significant.

Results

Vascular nesfatin-1 expression is upregulated under calcifying conditions

To determine the role of nesfatin-1 in ectopic calcification, we examined the levels of nesfatin-1 in calcific VSMCs and aortas, as well as in serum samples in patients with coronary calcification. Therefore, we established VSMC mineralization by osteogenic media containing Na_2HPO_4/NaH_2PO_4 solution (2.6 mM, high Pi) or the mixture of Ca^{2+} (2.5 mM) with β-glycerophosphate (β-GP, 5 mM), respectively. Compared with the control cells, the levels of nesfatin-1 were significantly upregulated in VSMCs upon exposure of high Pi (Fig. 1A-C). The phenomenon was replicated in VSMCs exposed to osteogenic medium (DMEM supplemented with 2.5 mM Ca^{2+} and 5 mM β-GP) (Fig. 1D-F). The abdominal aortas were cut into rings and cultured in DMEM or calcifying medium containing 3.8 mmol/L PO_4^{3-} solution for 7 days, and the expression of nesfatin-1 was examined. Similar to cellular results, western blotting, qPCR and immunofluorescence showed higher expression of nesfatin-1 in ex vivo aortas challenged by high Pi environment (Fig. 1G-I). It was shown that a negative correlation between α-SMA and nesfatin-1 expression in isolated aortas (Figure S1A). Likewise, the protein and mRNA levels of nesfatin-1 were concomitantly elevated in the aortic tissue of calcified mice compared to that of control mice (Fig. 1J-L). A linear regression analysis also unveiled that α-SMA was negatively correlative with nesfatin-1 expression in aortas from VD3-induced mice (Figure S1B). Serum levels of Nesfatin-1 were progressively augmented with the increasing severity of VC in enrolled subjects suffering from coronary artery calcification (Fig. 1M). Furthermore, a spearman correlation analysis revealed that serum nesfatin-1 levels were positive

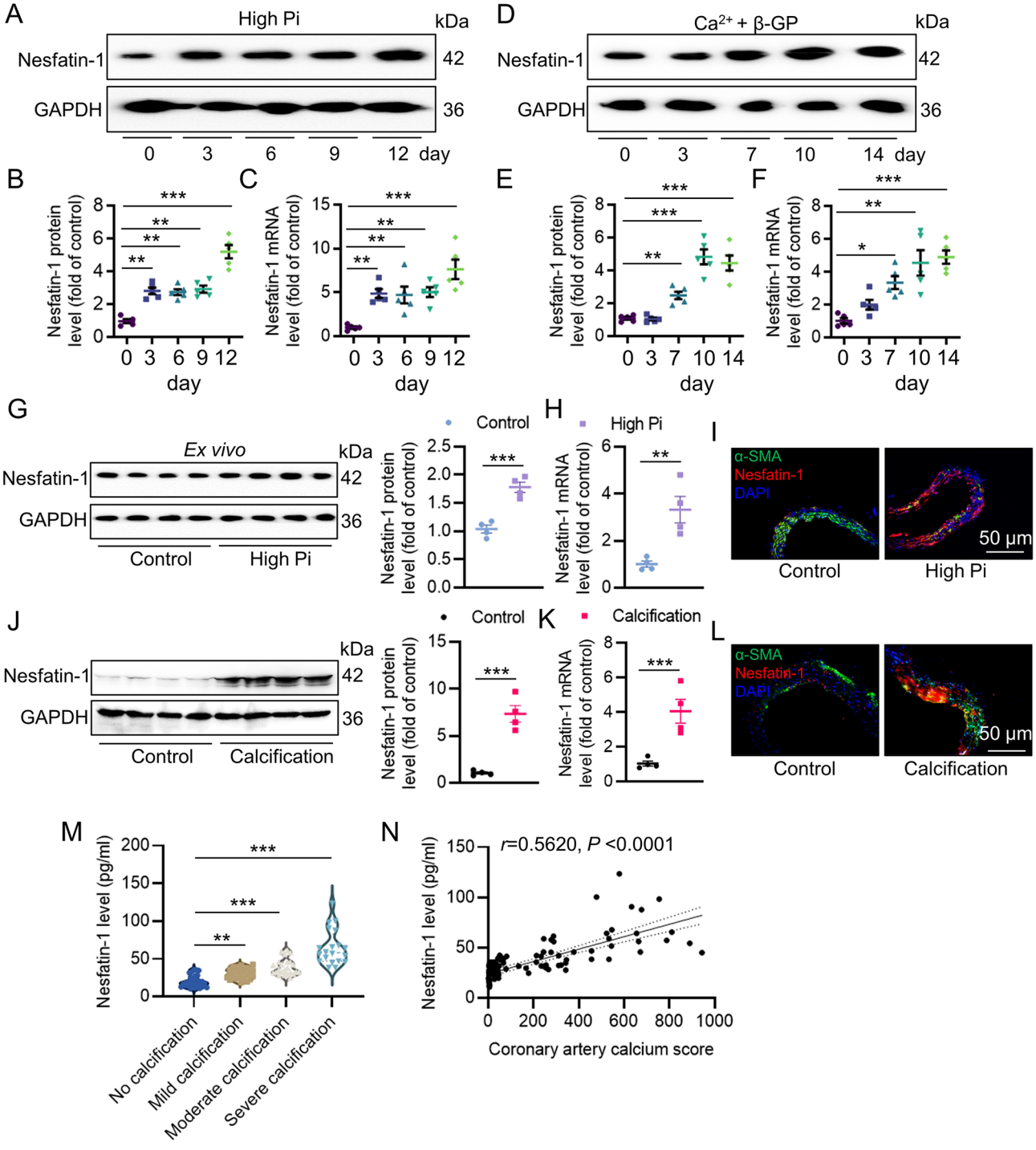

Fig. 1 Vascular nesfatin-1 expression is upregulated under calcifying conditions. (**A**, **B**) Western blot analysis of nesfatin-1 protein levels in VSMCs with high Pi (2.6 mM). (**C**) RT-PCR analysis of nesfatin-1 mRNA levels in VSMCs with high Pi (2.6 mM). (**D**, **E**) Western blot analysis of nesfatin-1 protein levels in VSMCs with β-GP (5 mM) and Ca^{2+} (2.5 mM). (**F**) RT-PCR analysis of nesfatin-1 mRNA levels in VSMCs with β-GP (5 mM) and Ca^{2+} (2.5 mM). (**G**) Western blot analysis of nesfatin-1 protein levels in isolated aortas with or without high Pi (3.8 mM) for 7 days. (**H**) RT-PCR analysis of nesfatin-1 mRNA levels in isolated aortas with or without high Pi (3.8 mM) for 7 days. (**I**) Immunofluorescence analysis of nesfatin-1 in isolated aortas with or without high Pi (3.8 mM) for 7 days. Scale bar, 50 μm. (**J**) Western blot analysis of nesfatin-1 protein levels in aortas from VD3-induced mice. (**K**) RT-PCR analysis of nesfatin-1 mRNA levels in from VD3-induced mice. (**L**) Immunofluorescence analysis of nesfatin-1 in isolated aortas from VD3-induced mice. Scale bar, 50 μm. (**M**) Serum levels of nesfatin-1 in different VC groups. (**N**) The positive association of serum nesfatin-1 levels with the coronary artery calcium scores by a Spearman correlation analysis. Differences between groups were assessed with ANOVA followed by Bonferroni post-hoc test (B-C, E-F, M). The P-value was calculated by unpaired two-tailed Student's t-test (G-H, J-K). The statistical significance of correlations was assessed by spearman's correlation coefficient analysis (N). $^{*}P<0.05$, $^{**}P<0.01$, $^{***}P<0.001$ versus the indicated group. $n=6$

correlative with the coronary artery calcium scores of patients (Fig. 1N).

Effects of nesfatin-1 on the progression of VC in vitamin D3 (VD3)-induced mice

To elucidate nesfatin-1 effects on the pathogenesis of VC, recombinant adeno-associated virus (AAV) encoding scrambled shRNA (shRNA-Ctrl) or nesfatin-1 shRNA (shRNA-Nesfatin-1) under the control of SM22α promoters was injected into VD3-induced medial arterial calcification mice via tail vein. The western blotting and mRNA results jointly confirmed the depletion of nesfatin-1 in the aortas (Fig. 2A-B). VSMC specific knockdown of nesfatin-1 ameliorated calcium deposition, as determined by calcium quantitative assay, ALP activity and alizarin red S staining (Fig. 2C-G). The protein expression of osteogenic proteins, RUNX2 and BMP-2, were increased, and the contractile proteins, α-SMA and SM22α, were notably lowered in the aortas of calcified mice, whereas nesfatin-1 deficiency reversed such abnormalities (Fig. 2H). As aforementioned, vitamin D injection dramatically enhanced the mRNA levels of RUNX2, Osterix, OPN and OCN in aortas, effects that were largely abolished by silencing nesfatin-1 (Fig. 2I). Contrary to the protein results, the upregulated BMP-2 mRNA level in calcifying aortas was not affected by knockdown of nesfatin-1 (Fig. 2I). To further ascertain these observations, we performed additional ex vivo aortic ring assays in the context of high Pi. As shown in Figure S2A-E, calcification of aortic ring was remarkably induced by high Pi stimulation, as demonstrated by von Kossa staining, calcium deposition and ALP activity. Conversely, nesfatin-1-deficient aortic explants exhibited lower calcification, along with lower RUNX2 mRNA level and higher α-SMA mRNA level (Figure S2F-G). In sharp contrast, overexpression of nesfatin-1 noticeably exacerbated calcification in both VD3-induced mice (Fig. 3) and high Pi-incubated aortic rings (Figure S2H-N). Therefore, the absence of smooth muscle specificity of nesfatin-1 relieved the pathologies of VC.

Effects of nesfatin-1 on osteogenic differentiation of VSMCs in vitro

To assess whether nesfatin-1 had an impact on the development of VC in VSMCs, we infected VSMCs with an adenovirus expressing shRNA-Ctrl or shRNA-Nesfatin-1, followed by high Pi treatment for 12 days. Nesfatin-1 shRNA3 was selected for our cellular experiments since Nesfatin-1 shRNA3 had the strongest ability to suppress the protein and mRNA levels of nesfatin-1 in VSMCs (Figure S4A-B). Nesfatin-1 deficiency negated high Pi-triggered increases in calcified nodule formation (Figure S4A), calcium content (Figure S4B) and ALP activity (Figure S4C). Nesfatin-1 downregulation lowered the protein expression of RUNX2 and BMP-2, while conserved the protein expression of α-SMA and SM22α in VSMCs treated with Pi (Figure S4D-E). In keeping with the animal results, disruption of nesfatin-1 maintained the mRNA levels of α-SMA and SM22α, whereas the mRNA levels of MSX2 and RUNX2 were lower in high Pi-treated VSMCs when nesfatin-1 was absent (Figure S4F). Similarly, downregulation of nesfatin-1 did not influence the mRNA level of BMP-2 in high Pi-stimulated VSMCs (Figure S4F). By contrast, nesfatin-1 overexpression potentiated osteogenic differentiation of VSMCs (Supplemental Figures S3C-D and S5). As such, nesfatin-1 may serve as a driver of VC by facilitating osteogenic transition of VSMCs. Interestingly, our findings indicate that BMP-2 signaling upregulated nesfatin-1 expression, suggesting a feedback loop that amplified VC (Figure S6). The nesfatin-1/BMP-2 complex mutually sustained their expression, forming a vicious cycle in VC.

Interaction of nesfatin-1 with BMP-2 induces BMP-2 osteogenic signaling

Among the numerous inducers of VC, BMP-2 is known to orchestrate both orthotopic bone formation and the osteoblastic differentiation of VSMCs. We next moved to ask whether nesfatin-1 promoted osteogenic transition of VSMCs by activating the osteogenic signaling of BMP-2. As depicted in Fig. 4A, treatment with a soluble form of bone morphogenetic protein receptor-type 1 A (BMPR-IA) effectively eliminated the actions of nesfatin-1 on the mRNA levels of osteochondrogenic markers, including Runx2, SOX9, Msx2, and α-SMA, implying the pro-calcifying effects of nesfatin-1 were dependent on BMP-2 signaling. In support, deletion of nesfatin-1 obviously impaired BMP-2-induced Smad phosphorylation, RUNX2/MSX2 expression, calcium content and ALP activity compared with those of scramble shRNA (Fig. 4B-D). Laser confocal photography showed the coexistence of nesfatin-1 with BMP-2 (Figure S7A). The co-IP results revealed a direct interaction between nesfatin-1 and BMP-2 (Figure S7B-C), and this interaction was enhanced in high Pi-incubated VSMCs (Figure S7D). To identify the specific fragments involved in this interaction, we generated truncated mutants of nesfatin-1 or BMP-2. Our results indicated that the 369–461 fragment of nesfatin-1 and the 284–395 fragment of BMP-2 mediate the interaction between these two proteins (Figure S7E-F). It had been shown that BMP-2 dissociates HDAC4 from RUNX2, leading to increased RUNX2 acetylation and transactivation [32]. The nuclear translocation of RUNX2 leads to calcium deposition in MC3T3-E1 cells [33], and is involved in the etiologies of calcific aortic valve disease [34]. The de-phosphorylation is a critical event for the nuclear translocation of HDAC4, leading to the FOXO deacetylation [35]. On these grounds, we

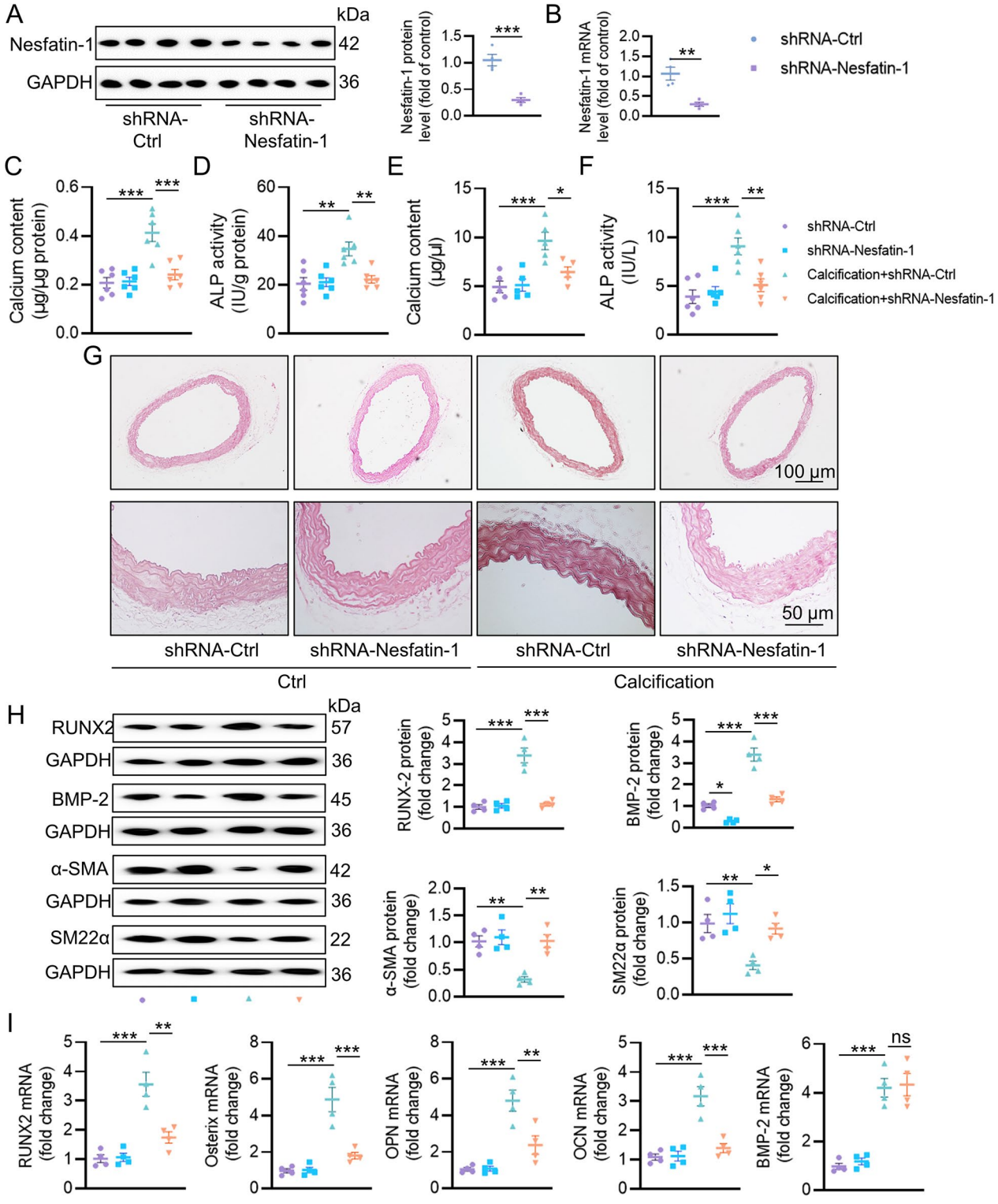

Fig. 2 Effects of nesfatin-1 knockdown on the progression of VC in VD3-induced mice. (**A**) Western blot analysis of nesfatin-1 protein levels in aortas. (**B**) RT-PCR analysis of nesfatin-1 mRNA levels in aortas. (**C**) Calcium content. (**D**) ALP activity. (**E**) Serum calcium content. (**F**) Serum ALP activity. (**G**) Representative Alizarin red S staining of aortas. Scale bar, 100 μm–50 μm. (**H**) Western blot analysis of RUNX2, BMP-2, α-SMA and SM22α. (**I**) RT-PCR analysis of RUNX2, Osterix, OPN, OCN, and BMP-2. The P-value was calculated by unpaired two-tailed Student's t-test (A-B). Differences between groups were assessed with ANOVA followed by Bonferroni post-hoc test (C-I). $^{*}P < 0.05$, $^{**}P < 0.01$, $^{***}P < 0.001$ versus the indicated group. $n = 6$

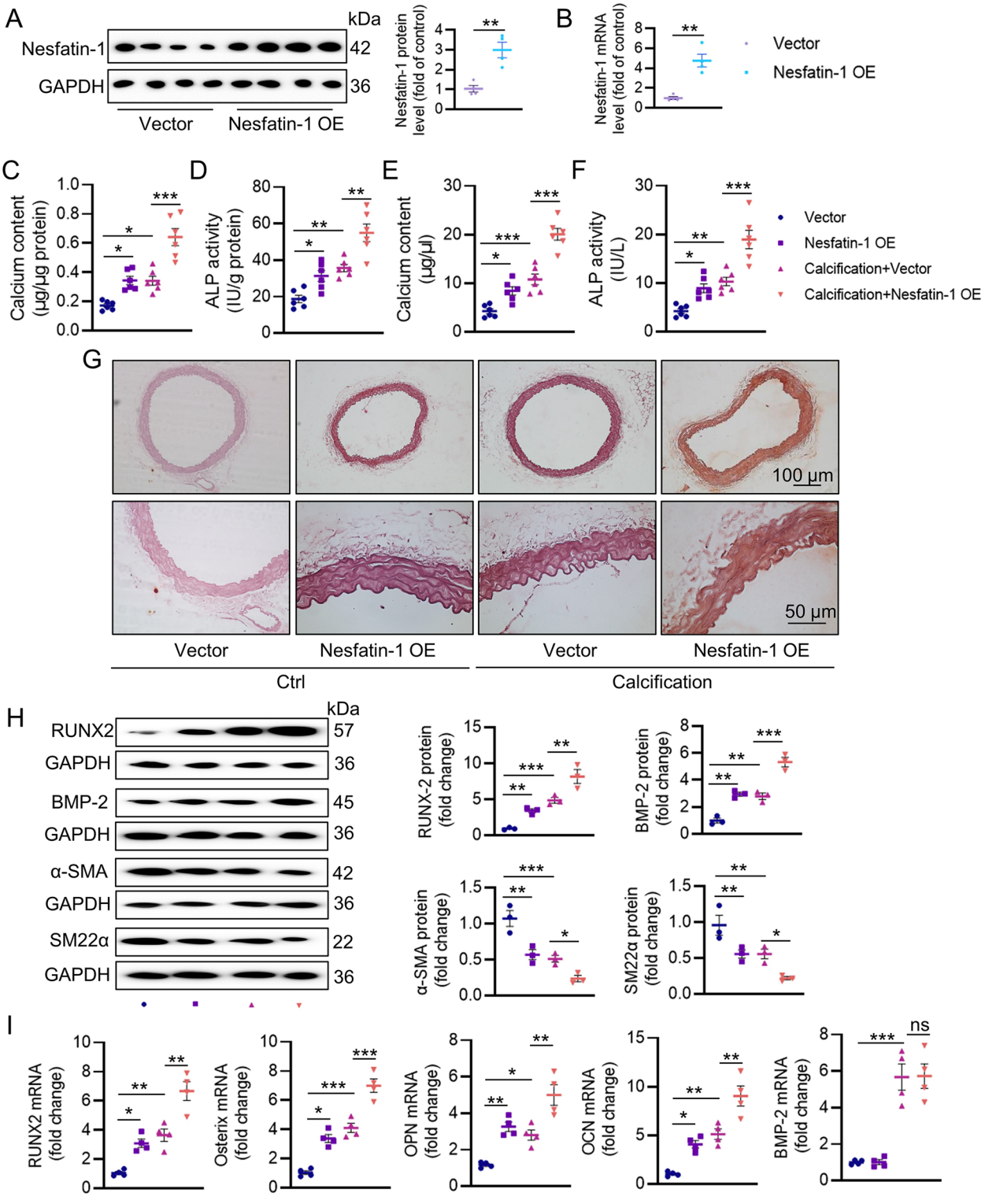

Fig. 3 Effects of nesfatin-1 overexpression on the progression of VC in VD3-induced mice. (**A**) Western blot analysis of nesfatin-1 protein levels in aortas. (**B**) RT-PCR analysis of nesfatin-1 mRNA levels in aortas. (**C**) Calcium content. (**D**) ALP activity. (**E**) Serum calcium content. (**F**) Serum ALP activity. (**G**) Representative Alizarin red S staining of aortas. Scale bar, 100 μm–50 μm. (**H**) Western blot analysis of RUNX2, BMP-2, α-SMA and SM22α. (**I**) RT-PCR analysis of RUNX2, Osterix, OPN, OCN, and BMP-2. The P-value was calculated by unpaired two-tailed Student's t-test (A-B). Differences between groups were assessed with ANOVA followed by Bonferroni post-hoc test (C-I). $^{*}P<0.05$, $^{**}P<0.01$, $^{***}P<0.001$ versus the indicated group. $n=6$

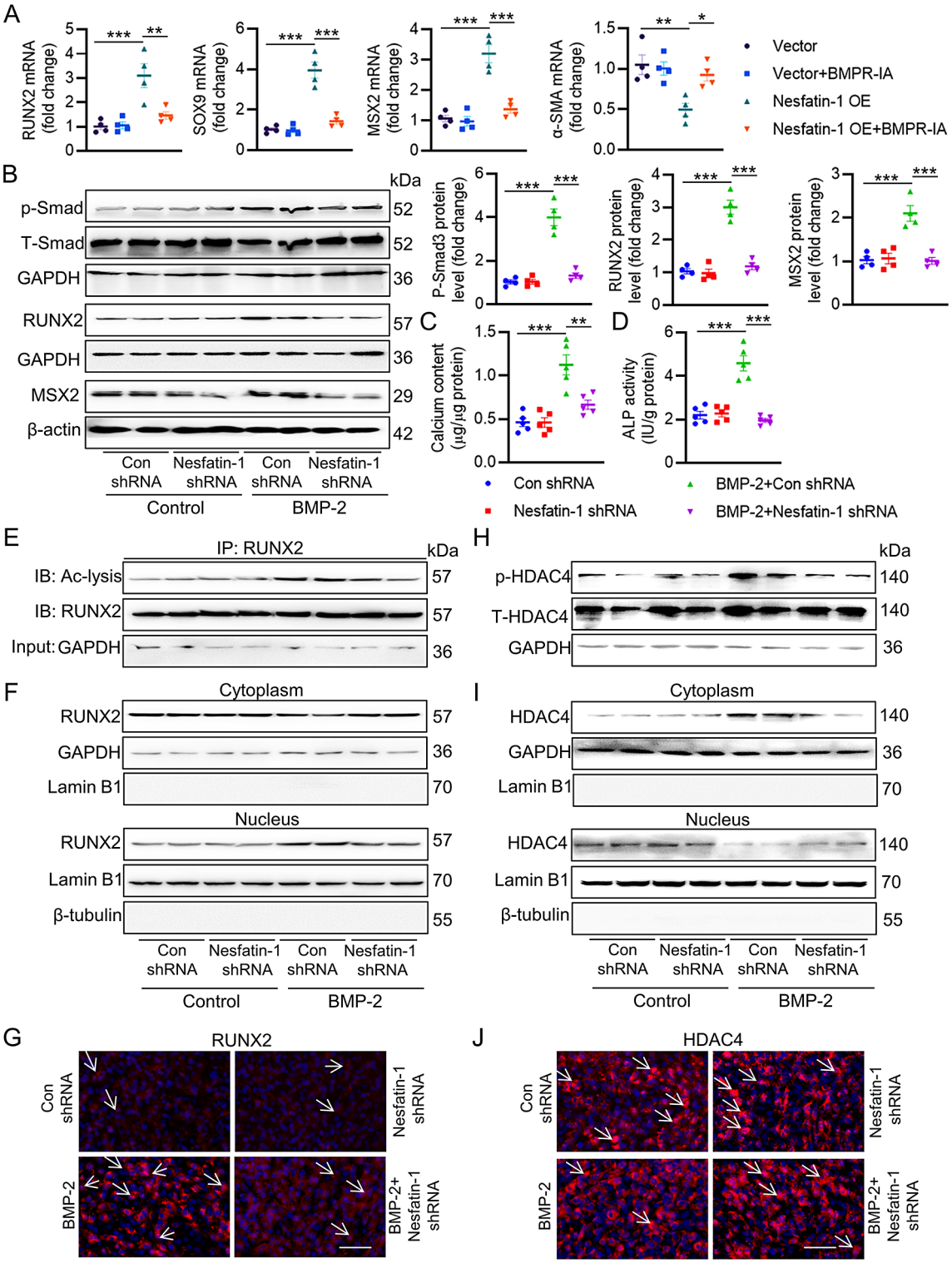

Fig. 4 Deletion of nesfatin-1 diminishes BMP-2 osteogenic signaling. (**A**) Quantitative RT-PCR analysis of RUNX2, SOX9, MSX2, α-SMA in VSMCs transfected with scramble vector or nesfatin-1 overexpression plasmid in the presence or absence of soluble BMPR-IA (1 mg/L). (**B**) Western blot analysis of Smad, RUNX2 and MSX2. (**C**) Quantification of calcium deposition. (**D**) ALP activity. (**E**) Acetylation level of RUNX2. (**F**) RUNX2 protein expression in the nucleus and cytoplasm. (**G**) Immunofluorescence staining of RUNX2. Scale bar, 25 μm. (**H**) The phosphorylation level of HDAC4. (**I**) HDAC4 protein expression in the nucleus and cytoplasm. (**J**) Immunofluorescence staining of HDAC4. Scale bar, 25 μm. Differences between groups were assessed with ANOVA followed by Bonferroni post-hoc test. *$P<0.05$, **$P<0.01$, ***$P<0.001$ versus the indicated group. $n=6$

hypothesized that nesfatin-1 knockdown might delay BMP-2-induced RUNX2 acetylation and nuclear translocation by inducing HDAC4 de-phosphorylation. As anticipated, BMP-2 stimulation promoted the acetylation and nuclear translocation of RUNX2, whereas this was strikingly inhibited by ablation of nesfatin-1 (Fig. 4E-G). Meanwhile, BMP-2-exposed VSMCs exhibited higher phosphorylation and nuclear exclusion of HDAC4, which were largely attenuated by downregulation of nesfatin-1 (Fig. 4H-J). Of note, the complex of HDAC4/RUNX2 was lower in VSMCs challenged by BMP-2, while nesfatin-1 knockdown restored their interaction (Figure S8A), leading to RUNX2 deacetylation and transcriptional inactivation. In conjunction with this, the binding of RUNX2 to OPN promoters was higher, while the HDAC4 located with OPN promoters was lower in VSMCs incubated with BMP-2. These abnormalities were reversed by deficiency of nesfatin-1 (Figure S8B-C). Conversely, nesfatin-1 overexpression held the opposite effects (Figure S9).

Nesfatin-1 triggers BMP-2 deubiquitination, stabilization and activation

As mentioned above, nesfatin-1 might regulate BMP-2 protein expression through the posttranslational modification because of our observations that nesfatin-1 did not affect the mRNA level of BMP-2 in VSMCs. It was found that the proteasome inhibitor MG-132, but not the autophagy-lysosome inhibitor chloroquine, prevented the degradation of BMP-2 protein induced by nesfatin-1 shRNA (Fig. 5A-B), suggesting that nesfatin-1 stabilized BMP-2 through the proteasomal degradation pathway. The half-life experiments demonstrated continuous and rapid degradation of BMP-2 induced by nesfatin-1 shRNA in VSMCs when protein synthesis was inhibited by cycloheximide (Fig. 5C). In the meantime, downregulation of nesfatin-1 accelerated the ubiquitination of BMP-2, whereas overexpression of nesfatin-1 diminished this degradation (Fig. 5D-E). To explore the potential E3 ligases responsible for the proteasomal degradation of BMP-2, we utilized UbiBrowser, an integrated bioinformatics platform designed for predicting proteome-wide E3 substrate networks (http://ubibrowser.ncpsb.org). Designating BMP-2 as a substrate led to the identification of 8 predicted E3 ligases in this platform. Among the 8 predicted E3 ligases, the top five with the highest confidence scores were filtered and presented in a list (Figure S10A-B). To validate these E3 ligases associated with BMP-2, we overexpressed five of them (MARCHF1, SYTL4, ZB2, MARCHF3, and MARCHF8) and assessed the corresponding protein expression of BMP-2. Ectopic expression of SYTL4 caused a significant reduction in BMP-2 protein (Fig. 5F), and downregulation of SYTL4 by SYTL4 shRNA1 exerted an opposite effect (Fig. 5H-I). Interestingly, the complex of nesfatin-1/SYTL4 was formed, as evidenced by a co-IP assay (Fig. 5G). Consistently, the depletion of SYTL4 abolished nesfatin-1 deficiency-induced upregulation of BMP-2 ubiquitination (Fig. 6A, C) and degradation (Fig. 6B, D). The calcification medium promoted the interaction of nesfatin-1 with SYTL4 (Fig. 6E), but diminished the formation of SYTL4/BMP-2 complex (Fig. 6F), indicating that nesfatin-1 might competitively bind to SYTL4, reducing SYTL4-mediated ubiquitination of BMP-2 and inducing BMP-2 in VC. Moreover, SYTL4 overexpression eliminated nesfatin-1 overexpression-triggered calcium deposition and ALP activity (Fig. 6G). Importantly, silencing SYTL4 weakened the effects of nesfatin-1 deficiency on calcium deposition and ALP activity in the setting of high Pi (Fig. 6H). Next, we set to figure out the possible ubiquitination sites of BMP-2. According to the BDM-PUB database (http://bdmpub.biocuckoo.org/prediction.php), three lysine residues were proposed to mediate the ubiquitination of BMP-2 (Figure S11A). The suppressive effects of nesfatin-1 shRNA on calcium deposition and ALP activity were disappeared upon mutating K290 to alanine (Figure S11B-C), hinting that K290 may be identified to be the ubiquitination sites of BMP-2 in response to downregulation of nesfatin-1.

Identification of potential nesfatin-1 inhibitors that ameliorate VC

From the cellular and animal results, it is likely that nesfatin-1 may function as a promising target for VC therapy. For this reason, we screened a small molecule pool containing 171 natural flavonoids using a luciferase reporter gene assay on the basis of nesfatin-1 promoter activity. Results showed that a total of 91 compounds suppressed the luciferase report gene activities of nesfatin-1 by more than 70% (Figure S12A). Among the top 10 compounds, Curculigoside and Chebulagic acid exhibited strong and comparable ability to repress nesfatin-1 activity (Figure S12B-C). Accordingly, Curculigoside and Chebulagic acid downregulated the protein expression of nesfatin-1 in a dose-dependent manner (Figure S12D-E). Molecular docking illustrated the interaction between Curculigoside and nesfatin-1 with binding energy of −9.035 KJ/mol (Fig. 7A-B). The binding of Chebulagic acid to nesfatin-1 was evaluated by molecular docking, and their binding energy was calculated as −7.194 KJ/mol (Fig. 7C-D). The binding of Curculigoside and Chebulagic acid to nesfatin-1 was also validated by the cellular thermal shift assay (CETSA) and Drug Affinity Responsive Target Stability (DARTS) (Figure S13A-C). The potential role of Curculigoside and Chebulagic acid in VC was then assessed. In calcified VSMCs, the calcium contents and ALP activity were significantly decreased after treatment with Curculigoside and Chebulagic acid (Figure S14A-C). We also observed that VSMCs treated with Curculigoside and

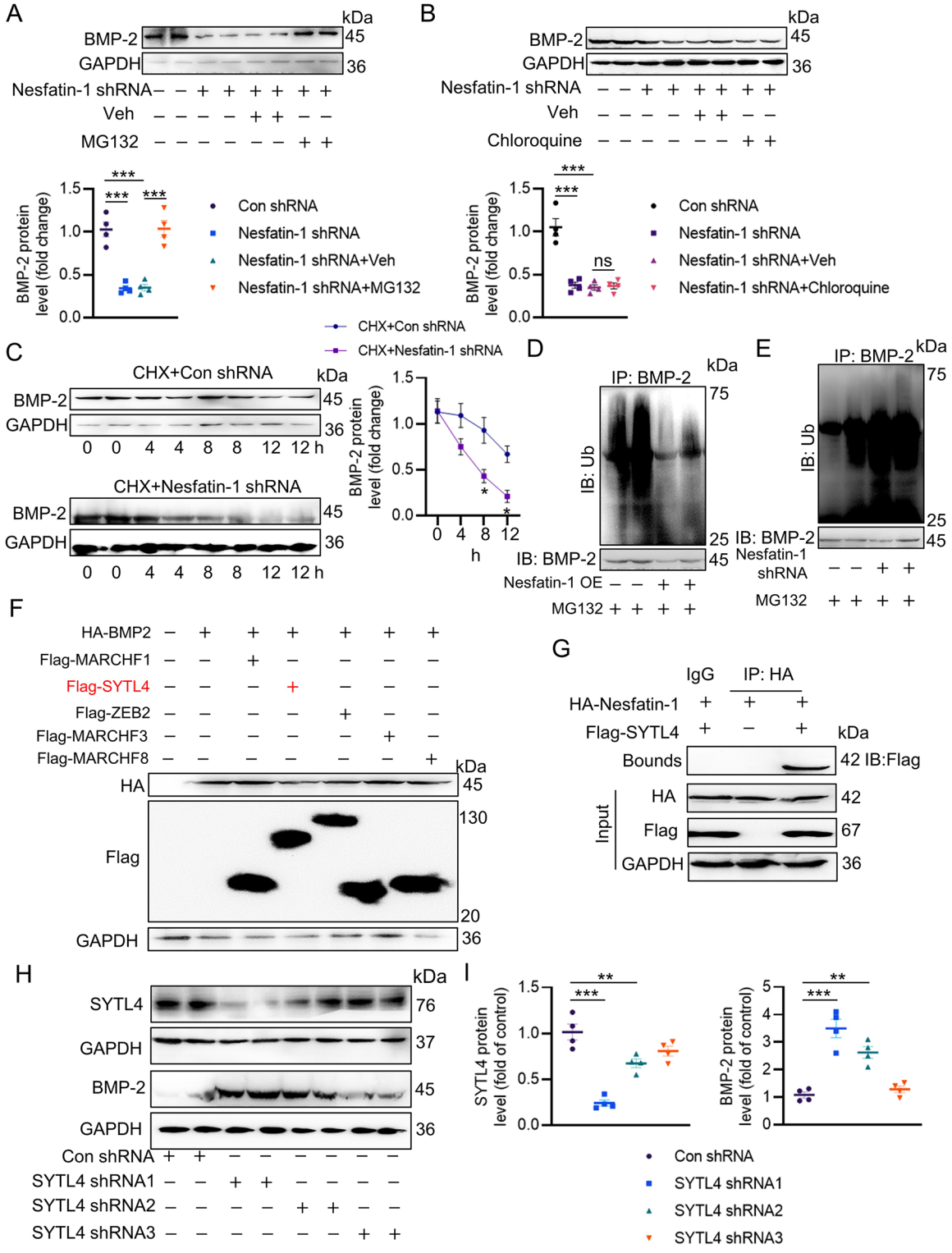

Fig. 5 Nesfatin-1 induces BMP-2 deubiquitination, stabilization and activation. (**A**) Quantitative Western blot analysis of BMP-2 in VSMCs in the presence of MG-132. (**B**) Quantitative Western blot analysis of BMP-2 in VSMCs in the presence of Chloroquine. (**C**) The half-life period of BMP-2. (**D**) Effects of nesfatin-1 overexpression on the ubiquitination of BMP-2. (**E**) Effects of nesfatin-1 knockdown on the ubiquitination of BMP-2. (**F**) Effects of MARCHF1, SYTL4, ZEB2, MARCHF3, and MARCHF8 overexpression on the protein expression of BMP-2. (**G**) Interaction of nesfatin-1 with SYTL4 by co-IP. (**H**, **I**) Effects of SYTL4 shRNA on the protein expression of SYTL4 and BMP-2. The P-value was calculated by unpaired two-tailed Student's t-test (**C**). Differences between groups were assessed with ANOVA followed by Bonferroni post-hoc test (**A**-**B**, **I**). $^{*}P < 0.05$, $^{**}P < 0.01$, $^{***}P < 0.001$ versus the indicated group. $n = 6$

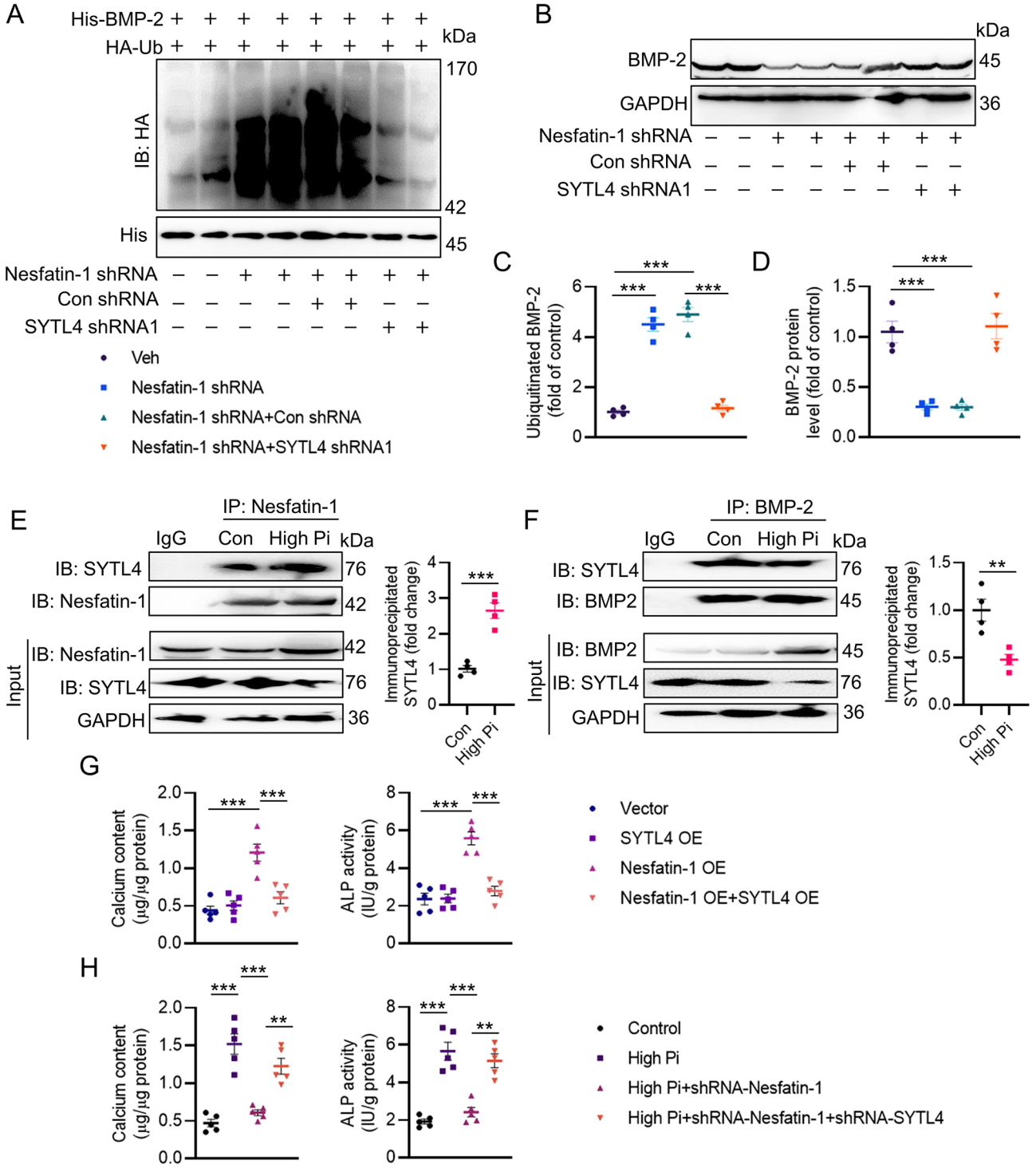

Fig. 6 SYTL4 contributes to BMP-2 ubiquitination and degradation. (**A**, **C**) Silencing SYTL4 abolished the effects of nesfatin-1 knockdown on the ubiquitination of BMP-2. (**B**, **D**) Silencing SYTL4 abolished the effects of nesfatin-1 knockdown on the protein expression of BMP-2. (**E**) High Pi increased the interaction of nesfatin-1 with SYTL4. (**F**) High Pi decreased the interaction of BMP-2 with SYTL4. (**G**) Overexpression of SYTL4 attenuated the deposition of calcium and ALP activity induced by nesfatin-1 overexpression. (**H**) Downregulation of SYTL4 attenuated the effects of nesfatin-1 deficiency on calcium deposition and ALP activity in VSMCs exposed to high Pi. Differences between groups were assessed with ANOVA followed by Bonferroni post-hoc test (C-D, G-H). The P-value was calculated by unpaired two-tailed Student's t-test (E-F). *$P<0.05$, **$P<0.01$, ***$P<0.001$ versus the indicated group. $n=6$

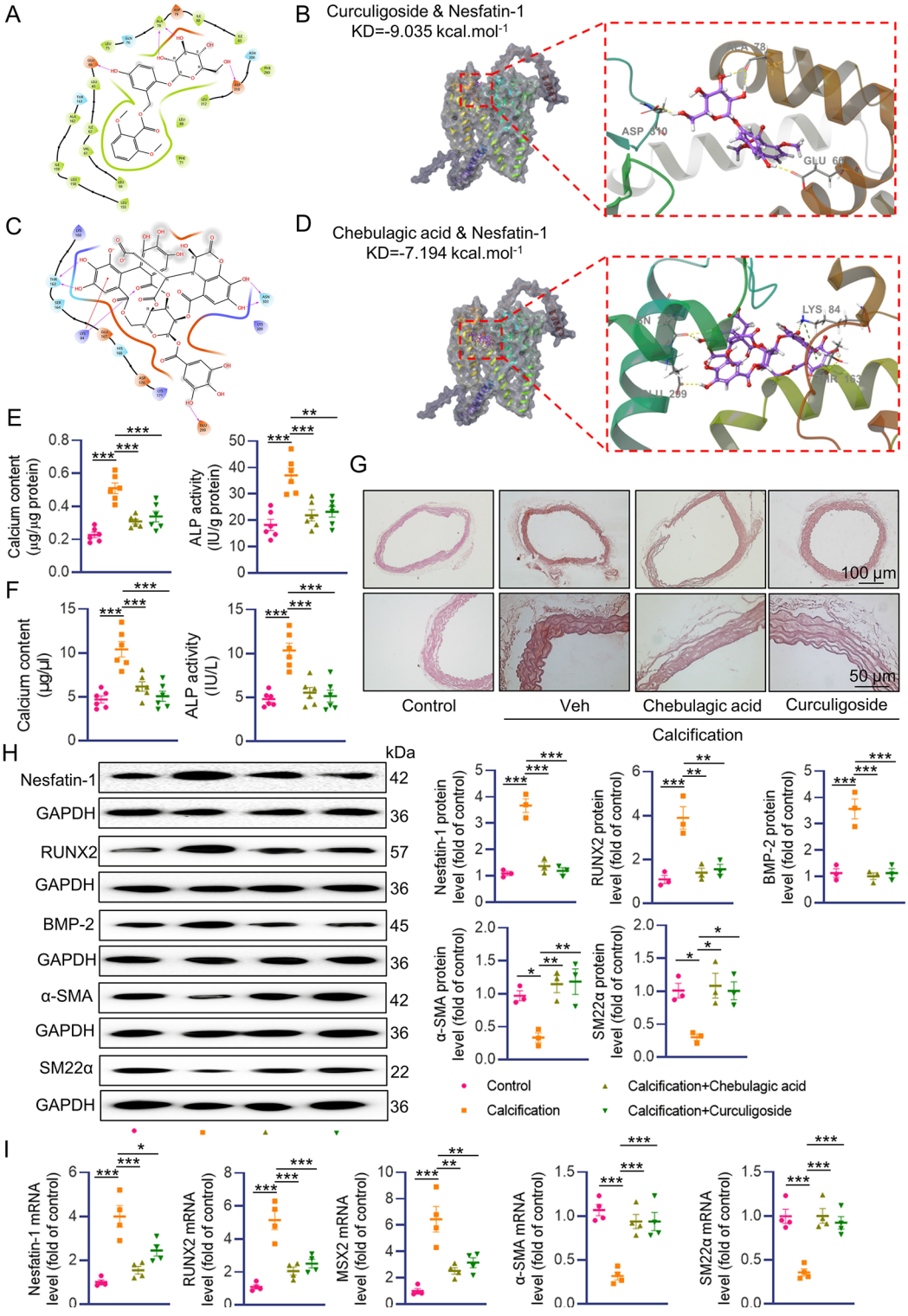

Fig. 7 Curculigoside and Chebulagic acid alleviated VC development in VD3-induced mice. (**A**, **B**) Molecular docking of nesfatin-1 with Curculigoside. (**C**, **D**) Molecular docking of nesfatin-1 with Chebulagic acid. (**E**) Calcium content and ALP activity in aortas. (**F**) Serum calcium content and ALP activity. (**G**) Representative Alizarin red S staining of aortas. Scale bar, 100 μm–50 μm. (**H**) Western blot analysis of nesfatin-1, RUNX2, BMP-2, α-SMA and SM22α. (**I**) RT-PCR analysis of nesfatin-1, RUNX2, MSX2, α-SMA and SM22α. Differences between groups were assessed with ANOVA followed by Bonferroni post-hoc test. *$P<0.05$, **$P<0.01$, ***$P<0.001$ versus the indicated group. $n=6$

Chebulagic acid displayed the downregulation of nesfatin-1, RUNX2, BMP-2 proteins, in conjunction with higher expression of α-SMA and SM22α (Figure S14D). This was further corroborated by RT-PCR results (Figure S14E). In consistence with cellular data, Curculigoside and Chebulagic acid treatment significantly reduced calcium content and ALP activity in both aortas and serum of VD3-induced mice (Fig. 7E-F). Alizarin-red S staining showed decreased calcium-phosphate salt deposition in VC aortas treated with Curculigoside and Chebulagic acid (Fig. 7G). As well, we found reduced protein expression of nesfatin-1, RUNX2 and BMP-2 in calcified aortas from mice subjected to Curculigoside and Chebulagic acid treatment (Fig. 7H). Conversely, the protein expression of α-SMA and SM22α was markedly upregulated in calcified aortas with Curculigoside and Chebulagic acid treatment (Fig. 7H). In addition, the abnormal mRNA levels of nesfatin-1, RUNX2, MSX2, α-SMA and SM22α in calcified aortas were counteracted after administration of Curculigoside and Chebulagic acid (Fig. 7I). Thus, downregulation of nesfatin-1 may be essential for Curculigoside and Chebulagic acid to curb VSMC calcification.

STAT3 occupies nesfatin-1 promoters and contributes to its upregulation in VC

To identify critical factors upregulating nesfatin-1 transcription, we designed DNA-protein screening experiments in VSMCs (Fig. 8A). From the MS results, we found that STAT3 was highly abundant from the promoter DNA-protein precipitates in VSMCs (Fig. 8B). We selected STAT3 as the transcription factor of interest because of its potential involvement in VSMC function, including VC [36, 37]. Indeed, the binding sites of STAT3 in nesfatin-1 promoters were predicted using JASPAR database (Fig. 8C, J). Overexpression of STAT3 actually promoted the protein expression of nesfatin-1, with concomitant increases in RUNX2 and BMP-2 proteins (Fig. 8D), vice versa (Fig. 8E). Additionally, STAT3 overexpression raised the luciferase reporter gene activity of nesfatin-1, while STAT3 downregulation inhibited it (Fig. 8F). More importantly, the enrichment of STAT3 within the nesfatin-1 promoters was higher in calcified aortas and VSMCs (Fig. 8G). Gene interference of STAT3 prevented the accumulation of calcium and ALP activity in VSMCs exposed to high Pi (Fig. 8H-I). As a consequence, STAT3 might directly bind to the nesfatin-1 promoters and boosted its transcription.

Disussion

In this study, we observed that the upregulation of nesfatin-1 contributed to the pathogenesis of VC. In support, the mice with VD3, aortas and primary VSMCs with high Pi incubation, showed higher expression of nesfatin-1. VSMC-specific nesfatin-1 overexpression aggravated VC in calcifying mice by potentiating the osteocyte transdifferentiation of VSMCs. By contrast, VSMC-specific nesfatin-1 downregulation reduced calcium deposit in aortas from arterial calcification mice. The substantial decrease in calcium deposition in aortic rings or VSMCs induced by calcification medium ex vivo or in vitro was observed by deficiency of nesfatin-1. Besides, nesfatin-1 reduced the ubiquitination degradation of BMP-2 by competitively binding to the E3 ligase SYTL4, resulting in the activation of BMP-2 signaling. Following this, BMP-2 induced phosphorylation of SMAD and HDAC4, the nuclear exclusion of HDAC4 increased acetylation and subsequent nuclear translocation of RUNX2 that promoted the transcription upregulation of MSX2, an important contributor to VC. We also revealed that the upregulation of nesfatin-1 may be mediated by STAT3 activation in VC. Eventually, we identified that Curculigoside and Chebulagic acid acted as potential inhibitors of nesfatin-1, leading to the amelioration of VC in vivo and in vitro. In summary, nesfatin-1 promotes osteochondrogenic differentiation of VSMCs and serves as a driver of VC, mediated at least in part via the deubiquitination and stabilization of BMP-2 (Fig. 9).

It has been disclosed that the serum level of nesfatin-1 is positively correlated with body mass index (BMI), hemoglobin A1c (HbA1c), and fasting blood glucose (FBG) in subjects with newly diagnosed type 2 diabetes mellitus [38]. The level of nesfatin-1 in the blood is positively correlated with the oxidative stress index in non-obese children with Prader–Willi syndrome [39]. Plasma nesfatin-1 levels are higher in patients with coronary artery disease and are associated with CAD independent of atherosclerotic risk factors, suggesting that higher nesfatin-1 levels may play a key role in the development of atherosclerosis [40]. Serum nesfatin-1 concentrations are closely related to the severity of acute myocardial infarction [41]. In patients with diabetes, those with microalbuminuria showed significantly elevated circulating levels of nesfatin-1 compared to normoalbuminuric patients [42]. Circulating nesfatin-1 levels appear to be linked to microalbuminuria regardless of other well-known risk factors for DKD [42]. Overexpression of nesfatin-1 induces hypertension and vascular remodeling [20, 43]. However, whether nesfatin-1 directly influenced the development of VC had not been explored before. In this study, we found higher levels of nesfatin-1 in the aortas of VD3-induced mice, and high Pi-incubated aortas, as well as primary VSMCs challenged by high Pi. Serum nesfatin-1 levels are associated with the increasing severity of VC in patients, and the prognostic significance of nesfatin-1 in VC warrants further studies. Notably, the expression of nesfatin-1 was higher in calcifying vessel tissues, likely reflecting local upregulation of nesfatin-1 in response to calcific stimuli, which may also be mirrored by increased

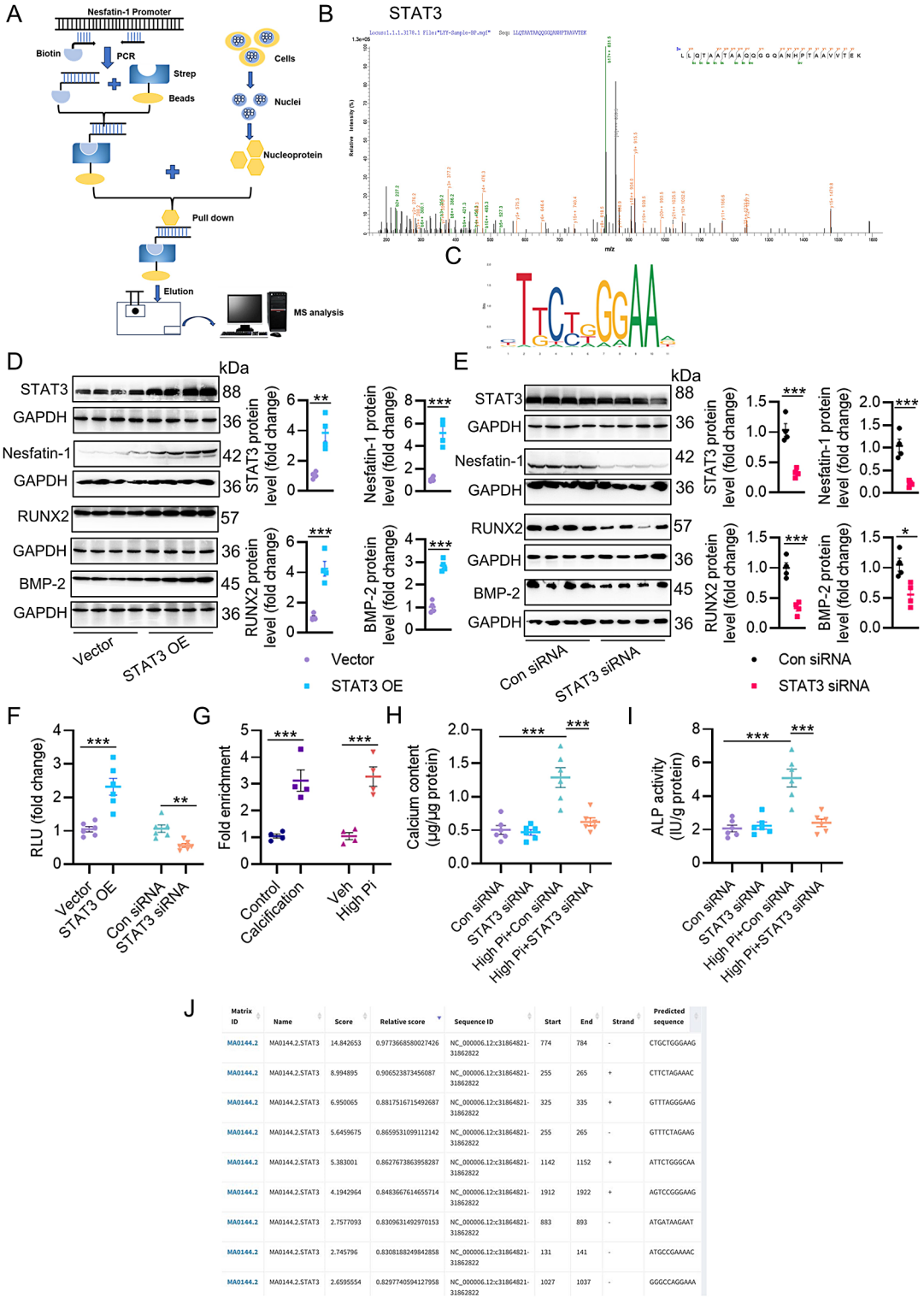

Matrix ID	Name	Score	Relative score	Sequence ID	Start	End	Strand	Predicted sequence
MA0144.2	MA0144.2.STAT3	14.842653	0.9773668580027426	NC_000006.12:c31864821-31862822	774	784	-	CTGCTGGGAAG
MA0144.2	MA0144.2.STAT3	8.994895	0.906523873456087	NC_000006.12:c31864821-31862822	255	265	+	CTTCTAGAAAC
MA0144.2	MA0144.2.STAT3	6.950065	0.8817516715492687	NC_000006.12:c31864821-31862822	325	335	+	GTTTAGGGAAG
MA0144.2	MA0144.2.STAT3	5.6459675	0.8659531099112142	NC_000006.12:c31864821-31862822	255	265	-	GTTTCTAGAAG
MA0144.2	MA0144.2.STAT3	5.383001	0.8627673863958287	NC_000006.12:c31864821-31862822	1142	1152	+	ATTCTGGGCAA
MA0144.2	MA0144.2.STAT3	4.1942964	0.8483667614655714	NC_000006.12:c31864821-31862822	1912	1922	+	AGTCCGGGAAG
MA0144.2	MA0144.2.STAT3	2.7577093	0.8309631492970153	NC_000006.12:c31864821-31862822	883	893	-	ATGATAAGAAT
MA0144.2	MA0144.2.STAT3	2.745796	0.8308188249842858	NC_000006.12:c31864821-31862822	131	141	-	ATGCCGAAAAC
MA0144.2	MA0144.2.STAT3	2.6595554	0.8297740594127958	NC_000006.12:c31864821-31862822	1027	1037	-	GGGCCAGGAAA

Fig. 8 STAT3 occupies nesfatin-1 promoters and contributes to its upregulation in VC. (**A**) Schematic of procedures for mass spectrometry (MS) screening in VSMCs. (**B**) Screening identified STAT3 bound to the nesfatin-1 promoters. m/z, mass/charge ratio. (**C**) The motif of STAT3 in Jaspar database. (**D**) Western blot analysis of STAT3, nesfatin-1, RUNX2, and BMP-2 after overexpression of STAT3. (**E**) Western blot analysis of STAT3, nesfatin-1, RUNX2, and BMP-2 after downregulation of STAT3. (**F**) Effects of STAT3 overexpression or downregulation on the luciferase reporter gene activity of nesfatin-1. (**G**) Fold enrichment of STAT3 within the promoters of nesfatin-1 in high Pi-incubated VSMCs or calcifying aortas. (**H**) Effects of STAT3 downregulation on calcium deposition in VSMCs incubated with high Pi. (**I**) Effects of STAT3 downregulation on ALP activity in VSMCs incubated with high Pi. (**J**) Predicted STAT3 and nesfatin-1 promoter binding regions. The P-value was calculated by unpaired two-tailed Student's t-test (D-G). Differences between groups were assessed with ANOVA followed by Bonferroni post-hoc test (H-I). $^{*}P < 0.05$, $^{**}P < 0.01$, $^{***}P < 0.001$ versus the indicated group. $n = 6$

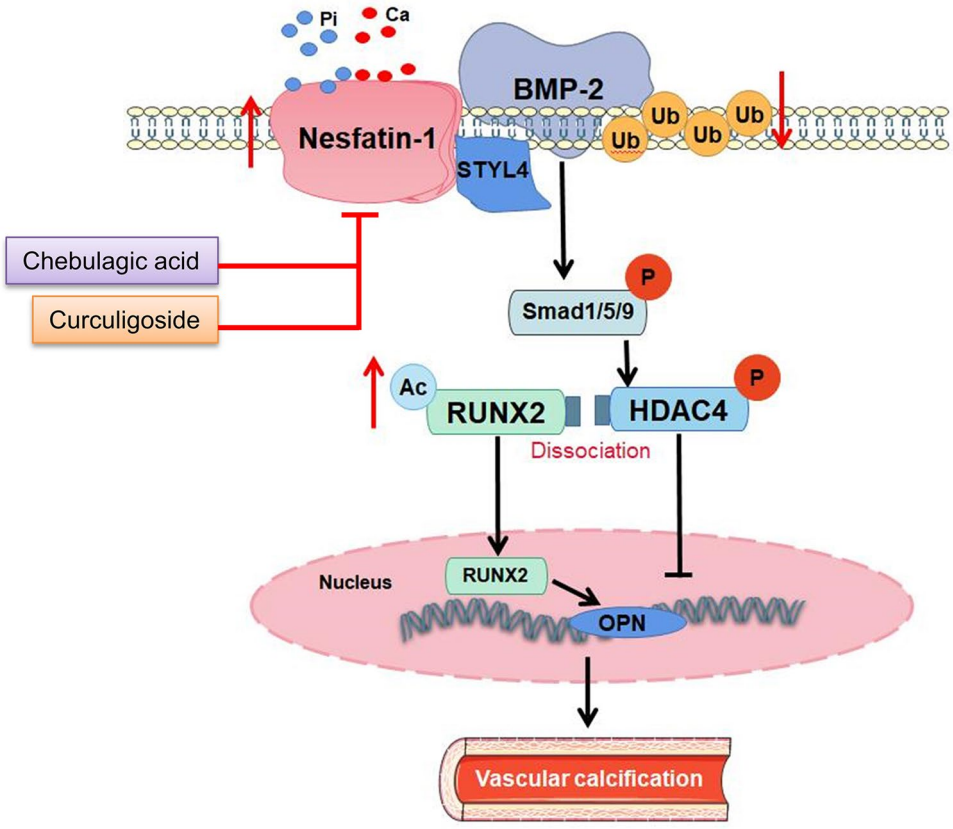

Fig. 9 Schematic illustration of the proposed mechanism of nesfatin-1 in the development of VC

serum nesfatin-1 levels due to systemic involvement. Due to the fact that nesfatin-1 is a neuropeptide, it is unknown whether calcification environment also promoted the release of nesfatin-1. This is a topic worth studying and is expected to be resolved in our future studies. Nesfatin-1, a hypothalamic-derived neuropeptide, plays a crucial role in regulating lipid metabolism under physiological conditions. However, its activity in promoting VC is likely modulated by several factors within the blood and the surrounding vascular microenvironment. The regulator role of nesfatin-1 in lipid metabolism suggests that its effects may be influenced by circulating lipoproteins, free fatty acids, and other lipid-related molecules. Elevated levels of LDL cholesterol, for example, could enhance the pro-calcific effects of nesfatin-1 by exacerbating lipid oxidation and promoting the formation of calcific nodules in VSMCs. Conversely, HDL cholesterol might counteract these effects by facilitating lipid efflux and reducing oxidative stress. Additionally, nesfatin-1 could interact with adipokines and cytokines in the blood, such as leptin and adiponectin, which are known to influence both lipid metabolism and inflammatory processes. The local microenvironment of the vasculature, including the presence of inflammatory cells, extracellular matrix components, and oxidative stress, may also modulate the activity of nesfatin-1. Inflammatory signaling, particularly via cytokines such as TNF-α and IL-6, could amplify nesfatin-1-induced VC. Moreover, oxidative stress, a hallmark of vascular calcification, may potentiate the pro-calcific effects of nesfatin-1 by promoting the differentiation of VSMCs into an osteogenic phenotype. The interplay between nesfatin-1 and these microenvironmental factors could also involve the modulation of signaling pathways such as NF-κB and MAPK, which may be critical in the regulation of inflammation and cellular stress responses. Thus, it is we proposed that the effects of nesfatin-1 on VC are not only direct but also influenced by the broader context of lipid metabolism, blood-borne inflammatory mediators, and the local vascular environment. These factors may collectively determine the extent to which nesfatin-1 contributes to the pathogenesis of VC, suggesting potential avenues for targeted therapeutic interventions. This viewpoint needs more experimental data, which deserved further studies.

VSMCs exhibit significant phenotypic plasticity when exposed to detrimental stimuli in their immediate environment. However, the underlying mechanisms that regulate the transformation of VSMCs into osteochondrogenic cells are not yet fully understood. Herein, we demonstrated that nesfatin-1 was involved in VSMC

osteogenic phenotypic switching since VSMCs with nesfatin-1 ablation were resistant to the transition to osteogenic-like cells, as demonstrated by Alizarin Red staining and calcium content detection. These findings were consistent with our previous observations that nesfatin-1 was essential to change the contractile phenotype of VSMCs [20, 21]. Thus, nesfatin-1 might play a procalcific role in the osteogenic differentiation of VSMCs. VC can manifest in the tunica intima, tunica media, or both layers of blood vessels. Intima calcification is typically observed in large arteriosclerotic plaques within larger arteries, while medial calcification (referred to as Monckeberg sclerosis) can affect arteries of varying sizes, characterized by diffuse mineral deposition along elastic fibers [44]. This type of calcification is commonly linked to chronic kidney disease (CKD), aging, and diabetes, whereas intimal calcification is associated with atherosclerotic lesions [45]. Aortic calcification and calcification in major branches are linked to vascular tissue stiffness and hypertension, conditions that heighten the risk of future cardiovascular events [46, 47]. Therefore, more studies are required to determine the potential role of nesfatin-1 in different animal models of VC.

BMP-2, traditionally acknowledged for its role in osteoblastic cell differentiation, is now also regarded as a key contributor to VC [48]. BMP-2 leads to the phosphorylation of regulatory Smad1/5/8 proteins, subsequently increasing the expression of key osteogenic transcription factors like Runx2 and Msx2 [49]. In the present study, we found that nesfatin-1 altered the protein of BMP-2 in the absence or presence of high Pi rather than the transcriptional level of BMP-2, indicating the regulatory role of nesfatin-1 in BMP-2 in a manner that dependent on a posttranslational modification. We further found that nesfatin-1 triggered the deubiquitinated and stabilized the protein expression of BMP-2 by isolating the E3 ligase SYTL4 from BMP-2. Nesfatin-1 physically interacted with BMP-2, and this interaction induced Smad phosphorylation, and upregulated the expression of the downstream transcriptional factors RUNX2 and MSX2. Accordingly, nesfatin-1 may modulate osteogenic transition of VSMCs by facilitating BMP-2 signaling. It should be mentioned that the role of SYTL4 in VC is rarely reported, and further studies are therefore acquired to investigate the contribution of SYTL4 to VC pathophysiology.

Gain- and loss-of-function assays demonstrated that HDAC4 is a positive regulator driving the process of VC [50]. HDAC4 could shuttle between the nucleus and cytoplasm in VSMCs, and the cytoplasmic HDAC4 is found to promote the progression of VC [50]. Thus, it is accepted that the cytoplasmic retention of HDAC4 is susceptible to the calcification process. RUNX2 is a primary target of the BMP-2 pathway, and genetic analysis has revealed that RUNX2 activity is suppressed by HDAC4 [32]. BMP-2 stimulated RUNX2 acetylation, and increased the transactivation activity and nuclear translocation of RUNX2 by inhibiting HDAC4 [32]. The phosphorylation of HDAC4 is indispensable for its sequestration in the cytoplasm, the dephosphorylation of HDAC4 potentiated the nuclear translocation of HDAC4 [35]. Collectively, on the one hand, BMP-2-induced Smad phosphorylation triggered the following HDAC4 phosphorylation, leading to cytoplasmic accumulation of HDAC4. On the other hand, BMP-2-induced Smad phosphorylation and resulted in the subsequent nuclear translocation of RUNX2. The dissociation of HDAC4 from the HDAC4/RUNX2 complex reduced RUNX2 deacetylation and hastened the transcriptional activity of RUNX2, thereby accelerating the initiation and development of VC. These events synergistically contributed to the positive effects of nesfatin-1 on VC development. In light of the importance of nesfatin-1 in VC, we found that Curculigoside and Chebulagic acid ameliorated VC by functioning as potential inhibitors of nesfatin-1. Also, the binding of STAT3 to nesfstin-1 contributed to nesfatin-1 upregulation during the process of VC. Thus, these results revealed the mechanisms that underlie the upregulation of nesfatin-1 in response to VC. In accordance, inhibiting nesfatin-1 had favorable effects on VC in vitro and in vivo. Of note, only VD3-induced mice were used in this study, further studies are warranted to clarify the role of nesfatin-1 in other models of VC, including genetic modifications, dietary changes, pharmacological interventions, or surgical procedures to induce calcification in the vascular tissues, such as atherosclerotic VC in Apolipoprotein E-deficient ($ApoE^{-/-}$) mice, Matrix Gla Protein-deficient ($MGP^{-/-}$) mice, klotho-deficient (kl/kl) mice, 5/6 nephrectomy rats, adenine-induced CKD rats, warfarin-induced calcification model, mice or rats fed with a high-fat diet or high-phosphate diet. It is noted that nesfatin-1 mitigates calcific aortic valve disease (CAVD) via suppressing ferroptosis in aortic valve interstitial cells . Nesfatin-1 appears to have opposite effects on aortic valve interstitial cells (AVICs) and vascular smooth muscle cells (VSMCs), which are critical cellular components in CAVD and VC, respectively. Heart valves and vascular tissues differ in their developmental origins, mechanical properties, and physiological functions, which may influence how cells within these tissues respond to nesfatin-1. For example, aortic valve interstitial cells may be more prone to undergoing osteogenic differentiation through oxidative stress and ferroptosis, while VSMCs respond to pro-calcific signals via osteogenic signaling cascades like BMP-2. The difference in nesfatin-1's effects in heart valve and vascular calcification can be attributed to tissue-specific cellular mechanisms and responses.

Understanding these distinct pathways is crucial for evaluating its potential as a therapeutic target and developing strategies that account for the context-dependent effects of nesfatin-1. STAT3 has been shown to regulate IL-1β, and Curculigoside and Chebulagic acid have anti-inflammatory effects. Further research is warranted to elucidate the specific mechanisms through which nesfatin-1 influences cytokine regulation and its implications in various pathological conditions.

Conclusion

We provide evidence that nesfatin-1 was associated with VC development and progression, and that it enhanced VC and the osteogenic differentiation of VSMCs through processes that involve the activation of BMP-2 signaling. Targeting nesfatin-1 may open up a promising approach for the prevention and treatment of VC in renal failure, hypertension, diabetes, and atherosclerosis. In future studies, we set to confirm the role of nesfatin-1 in VC using mice with VSMC-specific knockout or overexpression of nesfatin-1.

Supplementary Information

The online version contains supplementary material available at https://doi.org/10.1186/s12964-024-01873-7.

Supplementary Material 1

Supplementary Material 2

Acknowledgements
Not applicable.

Author contributions
QBL, JZ, ZJH, HBJ, HJS and XXZ designed this study and drafted the paper. XXZ, XYM, GC, JBS, XF carried out the experimental work and data analysis. AJX, YL, XHH, HBQ, QYS, JYH, and ZLL primarily handled animal experiments, cellular experiments, data analysis and figure preparation. All authors revised the paper and approved the final version of the manuscript.

Funding
This work was supported by the National Natural Science Foundation of China (82300414, 823700364, 8217021262 and 81700364), Jiangsu Province Excellent Youth Fund (BK20240204), Jiangsu Natural Science Foundation (BK20231049, BK20170179, BE2020634 and BK20191138), high-level introduction of talents and scientific research start-up funds of JNU (1286010241222100, 1286010241230530), the Fundamental Research Funds for the Central Universities (JUSRP124036), Jiangsu Province department of science and technology (BE2020634, BK20191138), Top Talent Support Program for young and middle-aged people of Wuxi Health Committee (BJ2020049) and Clinical Research and Translational Medicine Research Program of Affiliated Hospital of Jiangnan University (LCYJ202306, LCYJ202226), Wuxi Science and Technology Development Fund Project "Light of the Taihu Lake"(K20221028), Wuxi Municipal Health Commission Youth Project (Q202226), Wuxi City "Double Hundred" Young and Middle aged Medical and Health Top Talents Training Program Project (HB2023045), the Translational Medicine Project of the Wuxi Municipal Health Commission [ZH202107], Medical Discipline Program of Wuxi Health Commission, the Science and Technology Projects of Wuxi City (M202207, BJ2023029).

Data availability
No datasets were generated or analysed during the current study.

Declarations

Ethics approval and consent to participate
All animals were approved by the Care and Use of Laboratory Animals of China Pharmaceutical University (202101006). This study was adhered to the ethical principles outlined in the 1975 Declaration of Helsinki and received prior approval from the Ethics Committee of Nanjing Medical University (20180705-K048).

Consent for publication
Not applicable.

Competing interests
The authors declare no competing interests.

Author details
[1]MOE Medical Basic Research Innovation Center for Gut Microbiota and Chronic Diseases, School of Medicine, Jiangnan University, Wuxi 214122, China
[2]Department of Physiology, Eberhard-Karls-University of Tübingen, Tübingen University, Tübingen 72076, Germany
[3]Department of Anesthesiology, Affiliated Hospital of Jiangnan University, Jiangnan University, Wuxi 214122, China
[4]Department of Ultrasound, The Fourth Affiliated Hospital of Nanjing Medical University, Nanjing 210000, China
[5]State Key Laboratory of Natural Medicines, China Pharmaceutical University, No. 24 Tongjia Lane, Nanjing 210009, China
[6]Department of Cardiology, Wuxi No.2 People's Hospital (Jiangnan University Medical Center), Wuxi School of Medicine, Jiangnan University, Wuxi 214001, China
[7]Department of Clinical Research Center, Jiangnan University Medical Center (Wuxi No.2 People's Hospital), Wuxi School of Medicine, Jiangnan University, Wuxi 214001, China
[8]Department of Endocrinology, Affiliated Hospital of Jiangnan University, Jiangnan University, Wuxi 214122, China

Received: 1 July 2024 / Accepted: 3 October 2024
Published online: 11 October 2024

References

1. Turner ME, Beck L. Phosphate in Cardiovascular Disease: from New insights into Molecular mechanisms to clinical implications. Arterioscler Thromb Vasc Biol. 2024;44:584–602. https://doi.org/10.1161/atvbaha.123.319198.
2. Zhang T, Li H, Ouyang C, Cao G, Gao J, Wu J, Yang J, Yu N, Min Q, Zhang C, Zhang W. Liver kinase B1 inhibits smooth muscle calcification via high mobility group box 1. Redox Biol. 2021;38:101828. https://doi.org/10.1016/j.redox.2020.101828.
3. Lu Y, Meng L, Ren R, Wang X, Sui W, Xue F, Xie L, Chen A, Zhao Y, Yang J, et al. Paraspeckle protein NONO attenuates vascular calcification by inhibiting bone morphogenetic protein 2 transcription. Kidney Int. 2024. https://doi.org/10.1016/j.kint.2024.01.039.
4. Zhang T, Cao G, Meng X, Ouyang C, Gao J, Sun Y, Wu J, Min Q, Zhang C, Zhang W. Lethal giant larvae 1 inhibits smooth muscle calcification via high mobility group box 1. J Mol Cell Cardiol. 2020;142:39–52. https://doi.org/10.1016/j.yjmcc.2020.03.017.
5. Faleeva M, Ahmad S. Sox9 accelerates vascular aging by regulating Extracellular Matrix composition and stiffness. Circ Res. 2024;134:307–24. https://doi.org/10.1161/circresaha.123.323365.
6. Rogers MA, Bartoli-Leonard F, Zheng KH, Small AM, Chen HY. Major Facilitator Superfamily Domain containing 5 inhibition reduces lipoprotein(a) uptake and calcification in Valvular Heart Disease. Circulation. 2024;149:391–401. https://doi.org/10.1161/circulationaha.123.066822.
7. Han D, Zhou T, Li L, AVCAPIR:. A Novel Procalcific PIWI-Interacting RNA in calcific aortic valve disease. Circulation. 2024. https://doi.org/10.1161/circulationaha.123.065213.
8. Onnis C, Virmani R. Coronary artery calcification: current concepts and clinical implications. Circulation. 2024;149:251–66. https://doi.org/10.1161/circulationaha.123.065657.

9. van der Toorn JE, Vernooij MW, Ikram MA, Kavousi M, Bos D. Progression of arterial calcifications: what, where, and in whom? Eur Radiol. 2024. https://doi.org/10.1007/s00330-023-10566-7.
10. Dong QQ, Tu YC, Gao P, Liao QQ, Zhou P, Zhang H, Shu HP, Sun LL, Feng L, Yao LJ. SGK3 promotes vascular calcification via Pit-1 in chronic kidney disease. Theranostics. 2024;14:861–78. https://doi.org/10.7150/thno.87317.
11. Kang JH, Kawano T, Murata M, Toita R. Vascular calcification and cellular signaling pathways as potential therapeutic targets. Life Sci. 2024;336:122309. https://doi.org/10.1016/j.lfs.2023.122309.
12. Pelczyńska M, Miller-Kasprzak E. The role of Adipokines and Myokines in the pathogenesis of different obesity phenotypes-new perspectives. Antioxid (Basel). 2023;12. https://doi.org/10.3390/antiox12122046.
13. Dore R, Levata L, Lehnert H, Schulz C. Nesfatin-1: functions and physiology of a novel regulatory peptide. J Endocrinol. 2017;232:R45–65. https://doi.org/10.1530/joe-16-0361.
14. Stavileci B, Koldaş ZL. The relationship between Vaspin, Nesfatin-1 plasma levels and presence of fragmented QRS with the severity of coronary atherosclerosis. Adv Med Sci. 2022;67:298–303. https://doi.org/10.1016/j.advms.2022.07.005.
15. Altas M, Uca AU. Serum levels of irisin and nesfatin-1 in multiple sclerosis. Arq Neuropsiquiatr. 2022;80:161–7. https://doi.org/10.1590/0004-282x-anp-2020-0520.
16. Wu X, Dai B, Yan F, Chen Y, Xu Y, Xia Q, Zhang X, Serum Cortisol. Nesfatin-1, and IL-1β: potential diagnostic biomarkers in Elderly patients with treatment-resistant depression. Clin Interv Aging. 2022;17:567–76. https://doi.org/10.2147/cia.s361459.
17. Güneş H, Alkan Baylan F. Can Nesfatin-1 predict hypertension in obese children? J Clin Res Pediatr Endocrinol. 2020;12:29–36. https://doi.org/10.4274/jcrpe.galenos.2019.2019.0072.
18. Kadim BM, Hassan EA. Nesfatin-1 - as a diagnosis regulatory peptide in type 2 diabetes mellitus. J Diabetes Metab Disord. 2022;21:1369–75. https://doi.org/10.1007/s40200-022-01070-8.
19. Luo JJ, Wen FJ, Qiu D, Wang SZ. Nesfatin-1 in lipid metabolism and lipid-related diseases. Clin Chim Acta. 2021;522:23–30. https://doi.org/10.1016/j.cca.2021.08.005.
20. Lu QB, Wang HP, Tang ZH, Cheng H, Du Q, Wang YB, Feng WB, Li KX, Cai WW, Qiu LY, Sun HJ. Nesfatin-1 functions as a switch for phenotype transformation and proliferation of VSMCs in hypertensive vascular remodeling. Biochim Biophys Acta Mol Basis Dis. 2018;1864:2154–68. https://doi.org/10.1016/j.bbadis.2018.04.002.
21. Zhang JR, Lu QB, Feng WB, Wang HP, Tang ZH, Cheng H, Du Q, Wang YB, Li KX, Sun HJ. Nesfatin-1 promotes VSMC migration and neointimal hyperplasia by upregulating matrix metalloproteinases and downregulating PPARγ. Biomed Pharmacother. 2018;102:711–7. https://doi.org/10.1016/j.biopha.2018.03.120.
22. Chai M, Zhang HT, Zhou YJ, Ji QW, Yang Q, Liu YY, Zhao YX, Shi DM, Liu W, Yang LX, et al. Elevated IL-37 levels in the plasma of patients with severe coronary artery calcification. J Geriatr Cardiol. 2017;14:285–91. https://doi.org/10.11909/j.issn.1671-5411.2017.05.013.
23. Zhang K, Zhang Y, Feng W, Chen R, Chen J, Touyz RM, Wang J, Huang H. Interleukin-18 enhances vascular calcification and osteogenic differentiation of vascular smooth muscle cells through TRPM7 activation. Arterioscler Thromb Vasc Biol. 2017;37:1933–43. https://doi.org/10.1161/atvbaha.117.309161.
24. Zeng P, Yang J, Liu L, Yang X, Yao Z, Ma C, Zhu H, Su J, Zhao Q, Feng K, et al. ERK1/2 inhibition reduces vascular calcification by activating miR-126-3p-DKK1/LRP6 pathway. Theranostics. 2021;11:1129–46. https://doi.org/10.7150/thno.49771.
25. Bhat OM, Yuan X, Cain C, Salloum FN, Li PL. Medial calcification in the arterial wall of smooth muscle cell-specific Smpd1 transgenic mice: a ceramide-mediated vasculopathy. J Cell Mol Med. 2020;24:539–53. https://doi.org/10.1111/jcmm.14761.
26. Ha CM, Park S, Choi YK, Jeong JY, Oh CJ, Bae KH, Lee SJ, Kim JH, Park KG, Jun do Y, Lee IK. Activation of Nrf2 by dimethyl fumarate improves vascular calcification. Vascul Pharmacol. 2014;63:29–36. https://doi.org/10.1016/j.vph.2014.06.007.
27. Darambazar G, Nakata M, Okada T, Wang L, Li E, Shinozaki A, Motoshima M, Mori M, Yada T. Paraventricular NUCB2/nesfatin-1 is directly targeted by leptin and mediates its anorexigenic effect. Biochem Biophys Res Commun. 2015;456:913–8. https://doi.org/10.1016/j.bbrc.2014.12.065.
28. Sun H, Zhang F, Xu Y, Sun S, Wang H, Du Q, Gu C, Black SM, Han Y, Tang H. Salusin-β promotes vascular calcification via Nicotinamide Adenine Dinucleotide Phosphate/Reactive oxygen species-mediated klotho downregulation. Antioxid Redox Signal. 2019;31:1352–70. https://doi.org/10.1089/ars.2019.7723.
29. Gao C, Fu Y, Li Y, Zhang X, Zhang L, Yu F, Xu SS, Xu Q, Zhu Y, Guan Y, et al. Microsomal prostaglandin E Synthase-1-Derived PGE2 inhibits vascular smooth muscle cell calcification. Arterioscler Thromb Vasc Biol. 2016;36:108–21. https://doi.org/10.1161/atvbaha.115.306642.
30. Chin RM, Fu X, Pai MY, Vergnes L, Hwang H, Deng G, Diep S, Lomenick B, Meli VS, Monsalve GC, et al. The metabolite α-ketoglutarate extends lifespan by inhibiting ATP synthase and TOR. Nature. 2014;510:397–401. https://doi.org/10.1038/nature13264.
31. Yu J, Zhong B, Zhao L, Hou Y, Ai N, Lu JJ, Ge W, Chen X. Fighting drug-resistant lung cancer by induction of NAD(P)H:quinone oxidoreductase 1 (NQO1)-mediated ferroptosis. Drug Resist Updat. 2023;70:100977. https://doi.org/10.1016/j.drup.2023.100977.
32. Jeon EJ, Lee KY, Choi NS, Lee MH, Kim HN, Jin YH, Ryoo HM, Choi JY, Yoshida M, Nishino N, et al. Bone morphogenetic protein-2 stimulates Runx2 acetylation. J Biol Chem. 2006;281:16502–11. https://doi.org/10.1074/jbc.M512494200.
33. Molagoda IMN, Jayasingha J, Choi YH. Fermented Oyster Extract promotes insulin-like growth factor-1-Mediated Osteogenesis and Growth Rate. Mar Drugs. 2020;18. https://doi.org/10.3390/md18090472.
34. Éva Sikura K, Combi Z, Potor L, Szerafin T, Hendrik Z, Méhes G, Gergely P, Whiteman M, Beke L, Fürtös I, et al. Hydrogen sulfide inhibits aortic valve calcification in heart via regulating RUNX2 by NF-κB, a link between inflammation and mineralization. J Adv Res. 2021;27:165–76. https://doi.org/10.1016/j.jare.2020.07.005.
35. Wang B, Moya N, Niessen S, Hoover H, Mihaylova MM, Shaw RJ, Yates JR 3rd, Fischer WH, Thomas JB, Montminy M. A hormone-dependent module regulating energy balance. Cell. 2011;145:596–606. https://doi.org/10.1016/j.cell.2011.04.013.
36. Han Y, Zhang J, Huang S, Cheng N, Zhang C, Li Y, Wang X, Liu J, You B, Du J. MicroRNA-223-3p inhibits vascular calcification and the osteogenic switch of vascular smooth muscle cells. J Biol Chem. 2021;296:100483. https://doi.org/10.1016/j.jbc.2021.100483.
37. Zhao XK, Zhu MM, Wang SN, Zhang TT, Wei XN, Wang CY, Zheng J, Zhu WY, Jiang MX, Xu SW, et al. Transcription factor 21 accelerates vascular calcification in mice by activating the IL-6/STAT3 signaling pathway and the interplay between VSMCs and ECs. Acta Pharmacol Sin. 2023;44:1625–36. https://doi.org/10.1038/s41401-023-01077-8.
38. Zhang Z, Li L, Yang M, Liu H, Boden G, Yang G. Increased plasma levels of nesfatin-1 in patients with newly diagnosed type 2 diabetes mellitus. Exp Clin Endocrinol Diabetes. 2012;120:91–5. https://doi.org/10.1055/s-0031-1286339.
39. Gajewska J, Ambroszkiewicz J. Associations between Oxidant/Antioxidant status and circulating adipokines in non-obese children with prader-Willi Syndrome. Antioxid (Basel). 2023;12. https://doi.org/10.3390/antiox12040927.
40. Ibe S, Kishimoto Y, Niki H, Saita E, Umei T, Miura K, Ikegami Y, Ohmori R, Kondo K, Momiyama Y. Associations between plasma nesfatin-1 levels and the presence and severity of coronary artery disease. Heart Vessels. 2019;34:965–70. https://doi.org/10.1007/s00380-018-01328-3.
41. Kuyumcu A, Kuyumcu MS, Ozbay MB, Ertem AG, Samur G. Nesfatin-1: a novel regulatory peptide associated with acute myocardial infarction and Mediterranean diet. Peptides. 2019;114:10–6. https://doi.org/10.1016/j.peptides.2019.04.003.
42. Irannejad A, Ghajar A, Afarideh M, Khajeh E, Noshad S, Esteghamati S, Afshari K, Kahe F, Ganji M, Saadat M, et al. Association of peripheral nesfatin-1 with early stage diabetic nephropathy. Pathophysiology. 2017;24:17–22. https://doi.org/10.1016/j.pathophys.2016.12.001.
43. Mori Y, Shimizu H, Kushima H, Hiromura M, Terasaki M, Tanaka M, Osaki A, Hirano T. Increased blood pressure in nesfatin/nuclebindin-2-transgenic mice. Hypertens Res. 2017;40:861–7. https://doi.org/10.1038/hr.2017.61.
44. Vervloet MG, Adema AY, Larsson TE, Massy ZA. The role of klotho on vascular calcification and endothelial function in chronic kidney disease. Semin Nephrol. 2014;34:578–85. https://doi.org/10.1016/j.semnephrol.2014.09.003.
45. Wu M, Rementer C, Giachelli CM. Vascular calcification: an update on mechanisms and challenges in treatment. Calcif Tissue Int. 2013;93:365–73. https://doi.org/10.1007/s00223-013-9712-z.
46. Bashir A, Moody WE, Edwards NC, Ferro CJ, Townend JN, Steeds RP. Coronary artery Calcium Assessment in CKD: Utility in Cardiovascular Disease Risk Assessment and Treatment? Am J Kidney Dis. 2015;65:937–48. https://doi.org/10.1053/j.ajkd.2015.01.012.
47. Vlachopoulos C, Aznaouridis K, Stefanadis C. Prediction of cardiovascular events and all-cause mortality with arterial stiffness: a systematic review and

meta-analysis. J Am Coll Cardiol. 2010;55:1318–27. https://doi.org/10.1016/j.jacc.2009.10.061.
48. Hruska KA, Mathew S, Saab G. Bone morphogenetic proteins in vascular calcification. Circ Res. 2005;97:105–14. https://doi.org/10.1161/01.RES.0000175571.53833.6c.
49. Matilla L, Roncal C, Ibarrola J, Arrieta V, García-Peña A, Fernández-Celis A, Navarro A, Álvarez V, Gainza A, Orbe J, et al. A role for MMP-10 (Matrix Metalloproteinase-10) in calcific aortic valve stenosis. Arterioscler Thromb Vasc Biol. 2020;40:1370–82. https://doi.org/10.1161/atvbaha.120.314143.
50. Abend A, Shkedi O, Fertouk M, Caspi LH, Kehat I. Salt-inducible kinase induces cytoplasmic histone deacetylase 4 to promote vascular calcification. EMBO Rep. 2017;18:1166–85. https://doi.org/10.15252/embr.201643686.
51. Wang S, Gu J, Bian J, He Y, Xu X, Wang C, Li G, Zhang H, Ni B, Chen S, Shao Y, Jiang Y. Nesfatin-1 mitigates calcific aortic valve disease via suppressing ferroptosis mediated by GSH/GPX4 and ZIP8/SOD2 axes. Free Radic Biol Med. 2024 Sep;222:149-164. doi: 10.1016/j.freeradbiomed.2024.06.004. Epub 2024 Jun 7. PMID: 38851518.

Publisher's note